

AD-A168 718

SIMULATION ANALYSIS OF LOW FREQUENCY GROUND MOTIONS

1/1

OBSERVED FROM SELECTE. (U) S-CUBED LA JOLLA CA

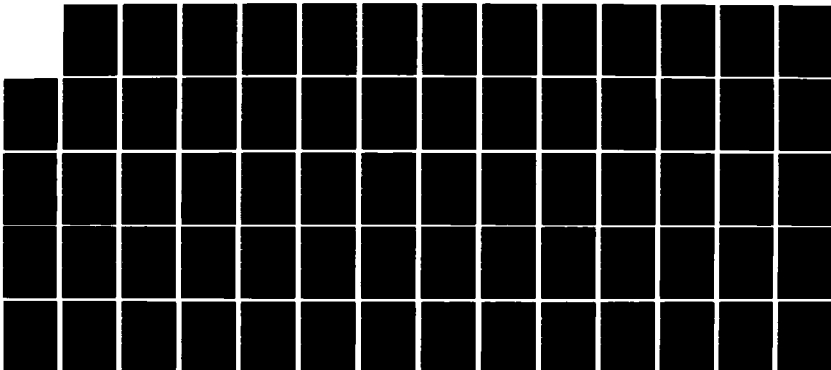
J R MURPHY ET AL. 01 MAR 84 555-R-84-6585 DNA-TR-84-70

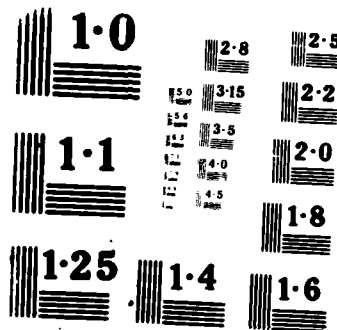
UNCLASSIFIED

DNA001-83-C-0136

F/G 18/3

NL





NATIONAL BUREAU  
MICROCOPY RESOLUTION

**AD-A168 718**

**DNA-TR-84-70**

# **SIMULATION ANALYSIS OF LOW FREQUENCY GROUND MOTIONS OBSERVED FROM SELECTED ATMOSPHERIC NUCLEAR EXPLOSIONS AT THE NEVADA TEST SITE**

**J. R. Murphy  
J. M. Dermengian  
H. K. Shah  
S-CUBED  
A Division of Maxwell Labs, Inc.  
P. O. Box 1620  
La Jolla, CA 92038-1620**

**1 March 1984**

**Technical Report**

**CONTRACT No. DNA 001-83-C-0136**

**Approved for public release;  
distribution is unlimited.**

THIS WORK WAS SPONSORED BY THE DEFENSE NUCLEAR AGENCY  
UNDER RDT&E RMSS CODE B344083466 Y99QAXSB00027 H2590D.

**Prepared for  
Director  
DEFENSE NUCLEAR AGENCY  
Washington, DC 20305-1000**

**DMC FILE COPY**

Destroy this report when it is no longer needed. Do not return to sender.

PLEASE NOTIFY THE DEFENSE NUCLEAR AGENCY,  
ATTN: STTI, WASHINGTON, DC 20305-1000, IF YOUR  
ADDRESS IS INCORRECT, IF YOU WISH IT DELETED  
FROM THE DISTRIBUTION LIST, OR IF THE ADDRESSEE  
IS NO LONGER EMPLOYED BY YOUR ORGANIZATION.



## DISTRIBUTION LIST UPDATE

This mailer is provided to enable DNA to maintain current distribution lists for reports. We would appreciate your providing the requested information.

- ☐ Add the individual listed to your distribution list.
- ☐ Delete the cited organization/individual.
- ☐ Change of address.

NAME: \_\_\_\_\_

ORGANIZATION: \_\_\_\_\_

### OLD ADDRESS

### CURRENT ADDRESS

\_\_\_\_\_  
\_\_\_\_\_  
\_\_\_\_\_

\_\_\_\_\_  
\_\_\_\_\_  
\_\_\_\_\_

TELEPHONE NUMBER: (    ) \_\_\_\_\_

SUBJECT AREA(s) OF INTEREST:

\_\_\_\_\_  
\_\_\_\_\_  
\_\_\_\_\_

\_\_\_\_\_  
\_\_\_\_\_  
\_\_\_\_\_

DNA OR OTHER GOVERNMENT CONTRACT NUMBER: \_\_\_\_\_

CERTIFICATION OF NEED-TO-KNOW BY GOVERNMENT SPONSOR (if other than DNA):

SPONSORING ORGANIZATION: \_\_\_\_\_

CONTRACTING OFFICER OR REPRESENTATIVE: \_\_\_\_\_

SIGNATURE: \_\_\_\_\_

Director  
Defense Nuclear Agency  
ATTN: STTI  
Washington, DC 20305-1000

Director  
Defense Nuclear Agency  
ATTN: STTI  
Washington, DC 20305-1000

UNCLASSIFIED

SECURITY CLASSIFICATION OF THIS PAGE

## REPORT DOCUMENTATION PAGE

1a. REPORT SECURITY CLASSIFICATION UNCLASSIFIED			1b. RESTRICTIVE MARKINGS		
2a. SECURITY CLASSIFICATION AUTHORITY N/A since Unclassified			3. DISTRIBUTION/AVAILABILITY OF REPORT  Approved for public release; distribution is unlimited.		
2b. DECLASSIFICATION/DOWNGRADING SCHEDULE N/A since Unclassified					
4. PERFORMING ORGANIZATION REPORT NUMBER(S) SSS-R-84-6585			5. MONITORING ORGANIZATION REPORT NUMBER(S) DNA-TR-84-70		
6a. NAME OF PERFORMING ORGANIZATION S-CUBED A Division of Maxwell Labs.		6b. OFFICE SYMBOL (If applicable)		7a. NAME OF MONITORING ORGANIZATION Director Defense Nuclear Agency	
6c. ADDRESS (City, State, and ZIP Code) P.O. Box 1620 La Jolla, CA 92038-1620			7b. ADDRESS (City, State, and ZIP Code) Washington, DC 20305-1000		
8a. NAME OF FUNDING/SPONSORING ORGANIZATION		8b. OFFICE SYMBOL (If applicable)		9. PROCUREMENT INSTRUMENT IDENTIFICATION NUMBER DNA 001-83-C-0136	
8c. ADDRESS (City, State, and ZIP Code)			10. SOURCE OF FUNDING NUMBERS		
			PROGRAM ELEMENT NO. 62715H	PROJECT NO. Y99QAXS	TASK NO. B
11. TITLE (Include Security Classification) SIMULATION ANALYSIS OF LOW FREQUENCY GROUND MOTIONS OBSERVED FROM SELECTED ATMOSPHERIC NUCLEAR EXPLOSIONS AT THE NEVADA TEST SITE					
12. PERSONAL AUTHOR(S) Murphy, J.R.; Dermengian, J.M.; and Shah, H.K.					
13a. TYPE OF REPORT Technical		13b. TIME COVERED FROM 830307 TO 840131		14. DATE OF REPORT (Year, Month, Day) 840301	
15. PAGE COUNT 66					
16. SUPPLEMENTARY NOTATION This Work was Sponsored by the Defense Nuclear Agency under RDT&E RMSS Code B344083466 Y99QAXSB00027 H2590D.					
17. COSATI CODES			18. SUBJECT TERMS (Continue on reverse if necessary and identify by block number)		
FIELD	GROUP	SUB-GROUP			
18	3		Ground Motion Simulation UPSHOT-KNOTHOLE 10		
8	11		Atmospheric Explosions TUMBLER I Pre-DIRECT COURSE		
			Surface Waves SMALL BOY Scaling Prediction		
19. ABSTRACT (Continue on reverse if necessary and identify by block number)					
<p>This report describes the results of a continuing investigation of the characteristics of the low frequency ground motions produced by atmospheric explosions. The studies reported here have focused on two aspects of this problem: (1) the full-scale validation of the adopted model through comparisons with ground motion data recorded from atmospheric nuclear tests, and (2) the preliminary evaluation of a theoretically-based prediction methodology.</p> <p>With regard to the validation study, the mathematical model has been applied to the theoretical simulation of ground motion data recorded from the Nevada Test Site atmospheric nuclear explosions TUMBLER I, UPSHOT-KNOTHOLE 10 and SMALL BOY. The results of these simulations have confirmed the fact that the observed low frequency ground motions from such explosions can be accounted for by the airblast-induced, elastic surface waves. Moreover,</p>					
20. DISTRIBUTION/AVAILABILITY OF ABSTRACT <input type="checkbox"/> UNCLASSIFIED/UNLIMITED <input checked="" type="checkbox"/> SAME AS RPT <input type="checkbox"/> DTIC USERS			21. ABSTRACT SECURITY CLASSIFICATION UNCLASSIFIED		
22a. NAME OF RESPONSIBLE INDIVIDUAL Betty L. Fox			22b. TELEPHONE (Include Area Code) (202) 325-7042		22c. OFFICE SYMBOL DNA/STTI

DD FORM 1473, 84 MAR

83 APR edition may be used until exhausted.  
All other editions are obsolete.

SECURITY CLASSIFICATION OF THIS PAGE

UNCLASSIFIED

UNCLASSIFIED

SECURITY CLASSIFICATION OF THIS PAGE

19. ABSTRACT (Continued)

the simulation analysis of the ground motion data recorded from the near-surface SMALL BOY explosion has confirmed the existence of an "exclusion radius" for such events, within which incident airblast energy is not efficiently coupled into the surface wave mode of propagation due to dissipation associated with strong, nonlinear interaction effects. On the other hand, the evidence provided by the TUMBLER I and UPSHOT-KNOTHOLE 10 analyses has indicated that this exclusion radius is effectively zero for explosions with significant height of burst.

In the prediction element of the study, the experience gained with the Pre-DIRECT COURSE experiment has been assessed and some approximate scaling laws describing the dependence of low frequency ground motion characteristics on variables such as yield, distance, site geology and instrument depth have been derived and discussed. It was shown that predicted surface wave characteristics are quite sensitive to the near-surface shear wave velocity structure at the site and that Pre-DIRECT COURSE experience indicates that this velocity distribution cannot be adequately constrained on the basis of P wave refraction surveys. For a given site, and for explosions which are large enough that the surface wave motions are dominated by frequency components near the corner frequency of the Rayleigh wave site response function, it has been shown that the theoretical model predicts that the amplitude of the low frequency ground motion should vary with yield,  $W$ , as  $W^{1/3}$  and with range,  $R$ , approximately as  $R^{-5/6}$ .

Accession For	
NTIS GRA&I	<input checked="checked" type="checkbox"/>
DTIC TAB	<input type="checkbox"/>
Unannounced	<input type="checkbox"/>
Justification	
By	
Distribution/	
Availability Codes	
Avail and/or	
Dist	Special



UNCLASSIFIED

SECURITY CLASSIFICATION OF THIS PAGE

# CONVERSION TABLE

Conversion factors for U.S. customary  
to metric (SI) units of measurement.

To Convert From	To	Multiply By
angstrom	meters (m)	1.000 000 X E -10
atmosphere (normal)	kilo pascal (kPa)	1.013 25 X E +2
bar	kilo pascal (kPa)	1.000 000 X E +2
barn	meter <sup>2</sup> (m <sup>2</sup> )	1.000 000 X E -28
British thermal unit (thermochemical)	joule (J)	1.054 350 X E +3
calorie (thermochemical)	joule (J)	4.184 000
cal (thermochemical)/cm <sup>2</sup>	mega joule/m <sup>2</sup> (MJ/m <sup>2</sup> )	4.184 000 X E -2
curie	giga becquerel (GBq)	3.700 000 X E +1
degree (angle)	radian (rad)	1.745 329 X E -2
degree Fahrenheit	degree kelvin (K)	$t_K = (t_F + 459.67)/1.8$
electron volt	joule (J)	1.602 19 X E -19
erg	joule (J)	1.000 000 X E -7
erg/second	watt (W)	1.000 000 X E -7
foot	meter (m)	3.048 000 X E -1
foot-pound-force	joule (J)	1.355 818
gallon (U.S. liquid)	meter <sup>3</sup> (m <sup>3</sup> )	3.785 412 X E -3
inch	meter (m)	2.540 000 X E -2
jerk	joule (J)	1.000 000 X E +9
joule/kilogram (J/kg) (radiation dose absorbed)	Gray (Gy)	1.000 000
kilotons	terajoules	4.183
kip (1000 lbf)	newton (N)	4.448 222 X E +3
kip/inch <sup>2</sup> (ksi)	kilo pascal (kPa)	6.894 757 X E +3
ktap	newton-second/m <sup>2</sup> (N-s/m <sup>2</sup> )	1.000 000 X E +2
micron	meter (m)	1.000 000 X E -6
mil	meter (m)	2.540 000 X E -5
mile (international)	meter (m)	1.609 344 X E +3
ounce	kilogram (kg)	2.934 952 X E -2
pound-force (lbs avoirdupois)	newton (N)	4.448 222
pound-force inch	newton-meter (N-m)	1.129 848 X E -1
pound-force/inch	newton/meter (N/m)	1.751 268 X E +2
pound-force/foot <sup>2</sup>	kilo pascal (kPa)	4.798 026 X E -2
pound-force/inch <sup>2</sup> (psi)	kilo pascal (kPa)	6.894 757
pound-mass (lbm avoirdupois)	kilogram (kg)	4.535 924 X E -1
pound-mass-foot <sup>2</sup> (moment of inertia)	kilogram-meter <sup>2</sup> (kg-m <sup>2</sup> )	4.214 011 X E -2
pound-mass/foot <sup>3</sup>	kilogram/meter <sup>3</sup> (kg/m <sup>3</sup> )	1.601 846 X E +1
rad (radiation dose absorbed)	*Gray (Gy)	1.000 000 X E -2
roentgen	coulomb/kilogram (C/kg)	2.579 760 X E -4
shake	second (s)	1.000 000 X E -8
slug	kilogram (kg)	1.459 390 X E +1
torr (mm Hg, 0° C)	kilo pascal (kPa)	1.333 22 X E -1

\*The becquerel (Bq) is the SI unit of radioactivity; 1 Bq = 1 event/s.

\*\*The Gray (Gy) is the SI unit of absorbed radiation.

## TABLE OF CONTENTS

<u>Section</u>	<u>Page</u>
CONVERSION TABLE . . . . .	iii
LIST OF ILLUSTRATIONS. . . . .	v
1 INTRODUCTION . . . . .	1
2 ANALYSIS of ATMOSPHERIC NUCLEAR EXPLOSION DATA: FULL SCALE VALIDATION . . . . .	3
2.1 MODEL DEFINITION. . . . .	3
2.2 SIMULATION ANALYSIS OF SELECTED ATMOSPHERIC NUCLEAR EXPLOSIONS AT NTS . . . . .	4
2.2.1 TUMBLER I. . . . .	8
2.2.2 UPSHOT-KNOTHOLE 10 . . . . .	14
2.2.3 SMALL BOY. . . . .	25
3 PREDICTION AND SCALING CONSIDERATIONS. . . . .	36
3.1 BACKGROUND. . . . .	36
3.2 Pre-DIRECT COURSE PREDICTIONS . . . . .	36
3.3 SCALING CONSIDERATIONS. . . . .	42
4 SUMMARY AND CONCLUSIONS. . . . .	49
4.1 SUMMARY . . . . .	49
4.2 CONCLUSIONS . . . . .	50
5 LIST OF REFERENCES . . . . .	53

# LIST OF ILLUSTRATIONS

<u>Figure</u>		<u>Page</u>
1	Subsurface geologic model for Frenchman Flat simulations . . .	6
2	Fundamental mode Rayleigh wave dispersion curves for Frenchman Flat model . . . . .	7
3	Fundamental mode Rayleigh wave site response function for Frenchman Flat model . . . . .	9
4	Comparison of observed (top) and synthetic (bottom) particle velocity waveforms for TUMBLER I. Vertical arrows denote predicted airblast arrival times . . . . .	10
5	Comparison of observed (top) with synthetic (bottom) air-slap-induced and Rayleigh wave vertical particle velocity waveforms for TUMBLER I, R = 482 m . . . . .	12
6	Comparison of fundamental and first higher mode Rayleigh wave contributions to vertical particle velocity waveforms for TUMBLER I, R = 407 m . . . . .	13
7	Vertical particle velocity waveforms for UPSHOT-KNOTHOLE 10. .	15
8	Comparison of unfiltered (top) and filtered (bottom) vertical particle velocity waveforms for UPSHOT-KNOTHOLE 10, R = 129 m . . . . .	16
9	Comparison of unfiltered (top) and filtered (bottom) vertical particle velocity waveforms for UPSHOT-KNOTHOLE 10, R = 432 m . . . . .	17
10	Comparison of unfiltered (top) and filtered (bottom) vertical particle velocity waveforms for UPSHOT-KNOTHOLE 10, R = 584 m . . . . .	18
11	Comparison of unfiltered (top) and filtered (bottom) vertical particle velocity waveforms for UPSHOT-KNOTHOLE 10, R = 736 m . . . . .	19
12	Comparison of unfiltered (top) and filtered (bottom) vertical particle velocity waveforms for UPSHOT-KNOTHOLE 10, R = 1041 m . . . . .	20
13	Comparison of observed and synthetic (fundamental mode) vertical particle velocity waveforms for UPSHOT-KNOTHOLE 10, R = 1041 m. Vertical arrow denotes predicted airblast arrival times . . . . .	22

# LIST OF ILLUSTRATIONS (Continued)

Figure		Page
14	Comparison of fundamental and first higher mode Rayleigh wave contributions to vertical particle velocity waveforms for UPSHOT-KNOTHOLE 10, $R = 1041$ m . . . . .	23
15	Comparison of observed and synthetic (fundamental plus first higher mode) vertical particle velocity waveforms for UPSHOT-KNOTHOLE 10, $R = 1041$ m. Vertical arrow denotes the predicted airblast arrival time . . . . .	24
16	Comparison of observed and synthetic (fundamental plus first higher mode) vertical particle velocity waveforms for UPSHOT-KNOTHOLE 10, $R = 736$ m. Vertical arrow denotes the predicted airblast arrival time . . . . .	26
17	Comparison of observed (top) and synthetic (bottom) vertical particle displacement waveforms for SMALL BOY at a range of 2139 m, Frenchman Flat subsurface model . . . . .	28
18	Comparison of observed (top) and synthetic (bottom) vertical particle displacement waveforms for SMALL BOY at a range of 2139 m, halfspace model . . . . .	29
19	Comparison of observed (top) and synthetic (bottom) vertical particle velocity waveforms for SMALL BOY at a range of 2139 m, halfspace model . . . . .	30
20	Comparison of composite synthetic velocity waveform (top) with contributions arising from loading of inner (30-100 m, center) and outer (100-1000 m, bottom) rings, SMALL BOY, $R = 2139$ m . . . . .	32
21	Comparison of observed vertical particle velocity waveform with synthetics computed using different values of the exclusion radius ( $R_0$ ), SMALL BOY, $R = 2139$ m . . . . .	34
22	Comparison of observed (top) and synthetic (bottom) vertical particle velocity waveforms for SMALL BOY at a range of 2139 m, halfspace model, linear tapering of the overpressure between 30 and 60 m . . . . .	35
23	Subsurface geologic model and associated fundamental mode Rayleigh wave dispersion curves, Pre-DIRECT COURSE . . . . .	37
24	Pre-DIRECT COURSE Rayleigh wave site response function ( $A_R$ ) . . . . .	39

# LIST OF ILLUSTRATIONS (Concluded)

<u>Figure</u>		<u>Page</u>
25	Comparison of predicted (top) and observed (bottom) vertical displacement waveforms for Pre-DIRECT COURSE, original site model . . . . .	40
26	Comparison of original and final subsurface models for Pre-DIRECT COURSE . . . . .	41
27	Comparison of predicted (top) and observed (bottom) vertical displacement waveforms for Pre-DIRECT COURSE, final site model . . . . .	43
28	Predicted variation of surface wave amplitude with depth for the special case $\beta_2/\beta_1 = 2$ , $\alpha = \sqrt{3} \beta$ , $f = \beta_1/2H$ . . . . .	47

## SECTION 1

### INTRODUCTION

As a result of research conducted in recent years, it is now well documented that the ground motion displacements observed from surface and atmospheric explosions outside the strong shock regime (i.e., at ranges where the peak incident overpressure has dropped below about 1000 kPa) are dominated by the low frequency, surface wave components of the motion (Murphy, 1978; Murphy and Bennett, 1980; Murphy et al., 1981; Murphy et al., 1982). It follows that in applications in which strategic system vulnerability at such ranges is an issue of concern, it is important that a reliable prediction capability be available for estimating the characteristics of these low frequency ground motions. Significant progress toward the development of such a capability has been achieved over the past several years, during which time a theoretical model has been formulated and successfully applied to the deterministic simulation of the low frequency ground motions observed from a variety of HE tests (e.g., Murphy, 1978; Murphy et al., 1981). However, some questions still remain concerning the extrapolation of this HE experience to the full scale nuclear environments which are of interest in ground motion assessment studies.

The objectives of the analyses described in this report have been to conduct a full scale validation study of the selected model using data recorded from atmospheric nuclear explosions at the Nevada Test Site (NTS) and to evaluate, in a preliminary fashion, the feasibility of employing a theoretically-based prediction methodology for routine applications. The results of the full scale validation study are presented in Section II, where the ground motions observed from three atmospheric nuclear explosions representing a wide range in scaled height of burst (HOB) are theoretically simulated by computing the surface wave response of models of the subsurface site geology to airblast loads predicted by the Speicher and Brode (1981) analytic approximations.

Some preliminary considerations concerning the prediction of low frequency ground motion parameters are addressed in Section III, where the experience gained with the Pre-DIRECT COURSE experiment is assessed and some approximate scaling laws describing the dependence of low

frequency ground motion characteristics on variables such as yield, distance, site geology and instrument depth are presented and discussed.

This is followed in Section IV by a summary, together with a statement of conclusions regarding our current state of knowledge concerning the low frequency ground motions produced by atmospheric explosions.

## SECTION 2

### ANALYSIS OF ATMOSPHERIC NUCLEAR EXPLOSION DATA: FULL SCALE VALIDATION

#### 2.1 MODEL DEFINITION.

The model which has been developed to simulate the low frequency ground motions observed from atmospheric explosions is based on the analytic solution for the elastic response of a multilayered model of the subsurface site geology to a propagating normal load acting on the surface (i.e., an approximation to an airblast). Assuming that the airblast load is axisymmetric, the Fourier transform of the Rayleigh wave component of the displacement for a particular mode at observation point  $\tilde{r}$ ,  $W(\omega, \tilde{r})$ , can be written as a spatial integration over the Fourier transform of the overpressure,  $p(r, \omega)$  in the form (Murphy and Bennett, 1980):

$$W(\omega, \tilde{r}) = -i\pi A_R(\omega) \left[ H_0^{(2)}(k\tilde{r}) \int_{r_0}^{\tilde{r}} p(r', \omega) J_0(kr') r' dr' \right. \\ \left. + J_0(k\tilde{r}) \int_{\tilde{r}}^{\infty} p(r', \omega) H_0^{(2)}(kr') r' dr' \right] \quad (1)$$

where  $A_R(\omega)$  is the Rayleigh wave site response function,  $J_0$ ,  $H_0^{(2)}$  denote the Bessel and Hankel functions respectively,  $k$  is the wavenumber of the Rayleigh wave component with frequency  $\omega$  and  $r_0$  denotes the exclusion radius which defines the region within which strong nonlinear effects occur. For surface bursts, it has been empirically determined that  $r_0$  coincides approximately with the crater radius. However, for atmospheric explosions with significant HOB (i.e., greater than  $r_0$ ), this heuristic approximation can be avoided and  $r_0$  is set to zero. For purposes of the present investigation, the airblast loading function,  $p(r, t)$ , has been specified using Brode's recently revised approximation (Speicher and Brode, 1981) which expresses the overpressure for a given yield ( $W$ ) and HOB as a function of range and time through products of functions involving fairly elaborate polynomial fits to the characteristics of airblasts observed

from surface and atmospheric nuclear explosions. The numerical procedures required to transform these time domain descriptions into the corresponding frequency domain representations required in the evaluation of Equation (1) (i.e.,  $p(r, \omega)$ ) have been described in detail by Murphy et al. (1982). Thus, given a multilayered approximation to the subsurface site geology and associated elastic parameters for each layer, the airblast-induced Rayleigh wave motions expected from atmospheric explosions of arbitrary yield and HOB can be calculated using equation (1).

## 2.2 SIMULATION ANALYSIS OF SELECTED ATMOSPHERIC NUCLEAR EXPLOSIONS AT NTS.

The analytical model described above has been successfully tested against data recorded from a variety of HE simulation tests (e.g., Murphy, 1978; Murphy et al., 1981). However, some questions still remain concerning the extrapolation of this HE experience to the full scale nuclear environments which are of interest in ground motion assessment studies. For this reason, a preliminary simulation analysis has been conducted in an attempt to test the analytical model against ground motion data measured from NTS atmospheric nuclear explosions. The events which have been selected for analysis are the TUMBLER I, UPSHOT-KNOTHOLE 10 and SMALL BOY explosions, all of which were detonated over the Frenchman Flat testing area at NTS. The characteristics of these explosions are summarized in Table 1 where it can be seen that they cover a wide range of scaled HOB extending from  $242 \text{ m/kt}^{1/3}$  to essentially zero. Thus, these tests provide an opportunity to assess simulation capability over essentially the entire range of potential interest in ground motion vulnerability studies.

The subsurface geological model of Frenchman Flat which has been adopted for initial simulation purposes is shown in Figure 1 (Sauer, 1958; Lipner, personal communication, 1981), where it can be seen that it is relatively simple, consisting of two layers over a halfspace. In this figure,  $\alpha$  and  $\beta$  denote the compressional and shear wave velocities and  $\rho$  the density. The fundamental mode Rayleigh wave dispersion curves corresponding to this site model are shown in Figure 2, and it can be seen that

Table 1. NTS explosion parameters\*.

Event	Date	Time GMT	Location		W, kt	HOB, m	$HOB/W_{1/3}^{1/3}$ , m/kt	Comment
			N.Lat.	W.Long.				
TUMBLER I (Able)	04-01-52	1700	36.7983	115.9356	1	242	242	Air Drop
UPSHOT-KNOTHOLE 10 (Grable)	05-25-53	1530	36.7931	115.9147	15	160	65	Fired from 280mm gun
SMALL BOY	07-14-62	1830	36.8025	115.9250	Low Yield	Slightly Above Ground	~ 0	Tower

\* Hawthorne, 1979

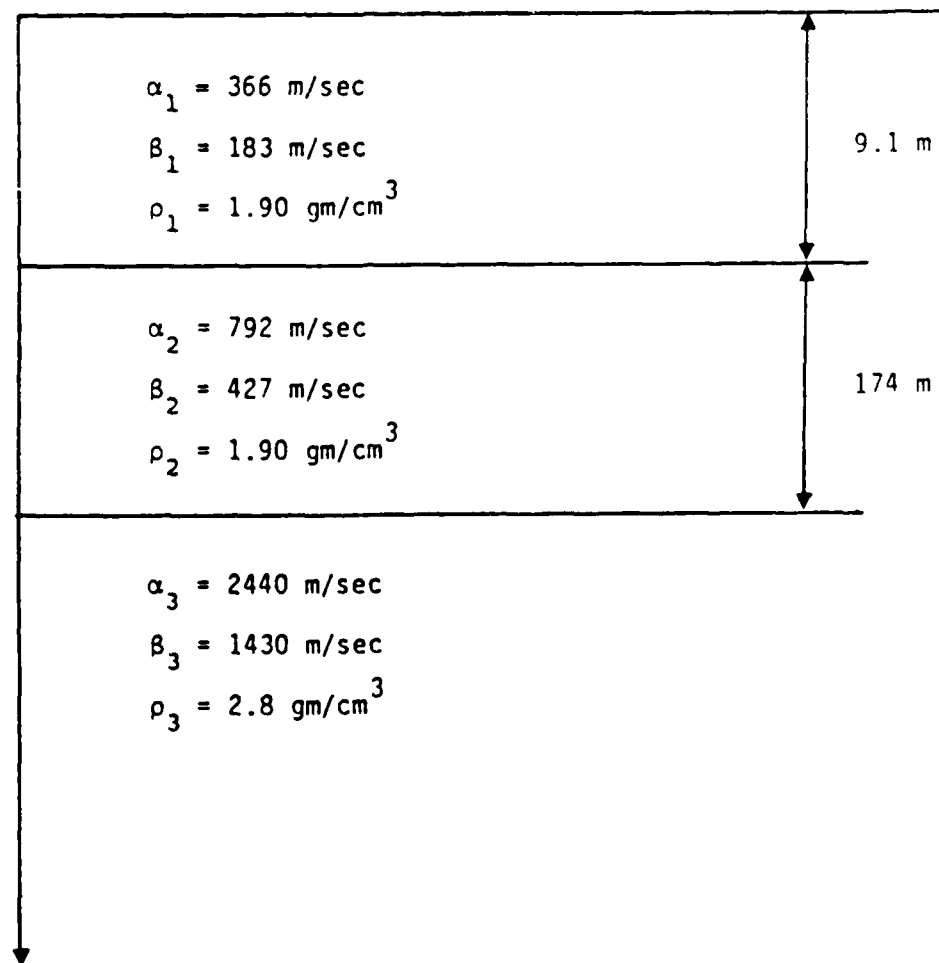


Figure 1. Subsurface geologic model for Frenchman Flat simulations.

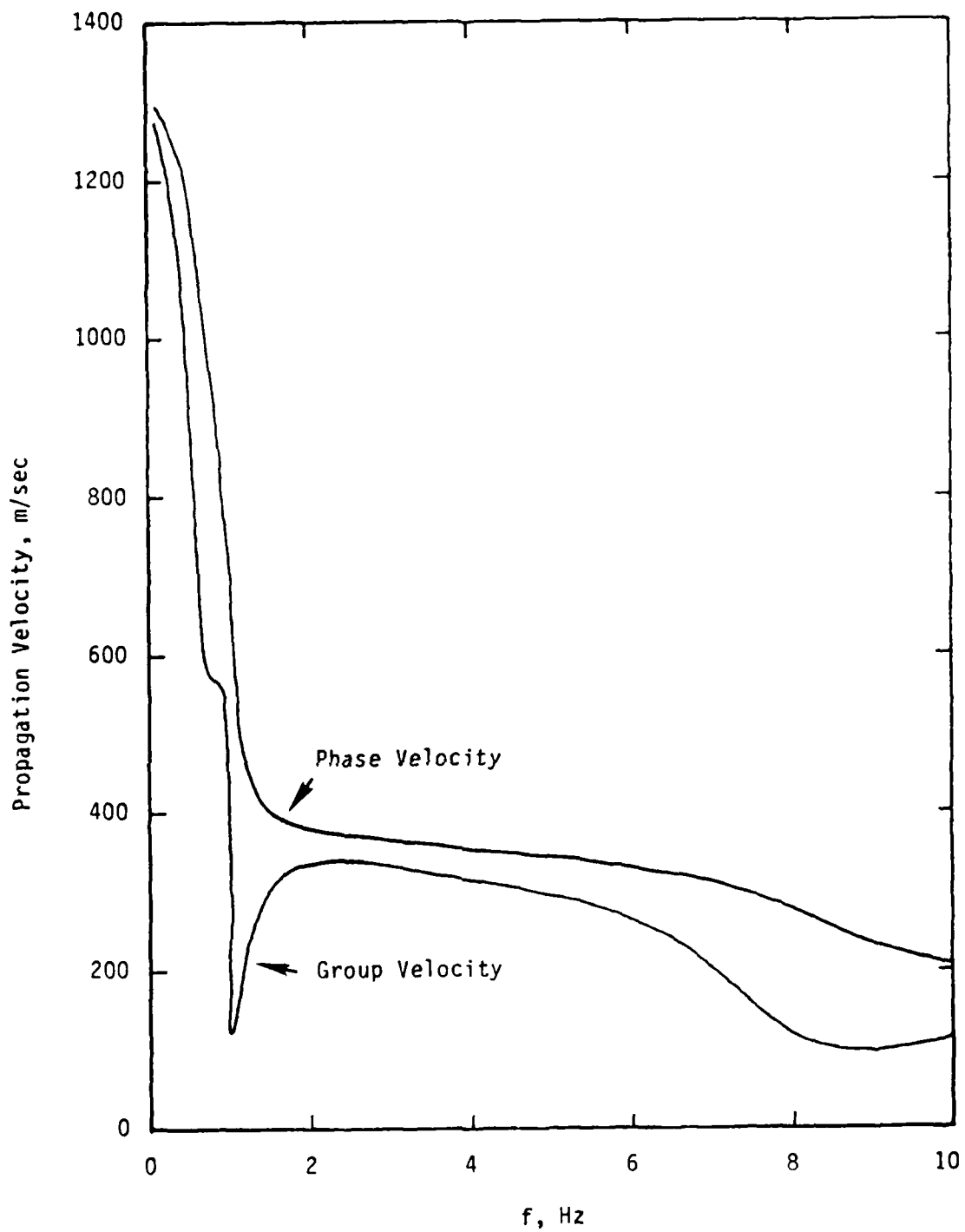


Figure 2. Fundamental mode Rayleigh wave dispersion curves for Frenchman Flat model.

there exists a very pronounced group velocity minimum at a frequency of about 1 Hz. Consequently, as is illustrated in Figure 3, the Rayleigh wave site response function (i.e.,  $A_R(\omega)$  in Equation (1)) drops off sharply for frequencies below 1 Hz. It follows that for explosions in the yield range of interest in the present investigation, it can be expected that the simulated low frequency ground motions will be dominated by components with frequencies of about 1 Hz (Murphy and Bennett, 1980).

#### 2.2.1 TUMBLER I.

Selected low frequency ground motions observed from this test have been simulated by analytically loading the surface of the geologic model of Figure 1 with an airblast loading function computed from the Speicher and Brode (1981) analytic approximation for a yield of 1 kt and an HOB of 242 m. In this case, the HOB is sufficiently large that no significant nonlinear effects are anticipated and  $r_0$  in Equation (1) is assumed to be zero. The TUMBLER I vertical particle velocity waveforms observed at ranges of 407 m, 482 m and 558 m are shown in Figure 4 where they are compared with the corresponding theoretical Rayleigh wave synthetic waveforms. It can be seen that the synthetics agree remarkably well with the observed waveforms up to the point where the observed data have been arbitrarily terminated during the data reduction. In particular, the dominant frequency content and amplitude level of the major low frequency pulse is reproduced to well within the typical data scatter. In fact, the only significant observed particle velocity which is not accounted for by the Rayleigh wave is the airslap-induced motion which is identified on Figure 4 by the vertical arrows which have been aligned with the predicted airblast arrival times at these ranges. In this overpressure regime ( $< 100$  kPa), the ground motion associated with this loading can be simulated with reasonable accuracy using a simple, linear one-dimensional model which incorporates the reverberation of energy within the surface layer. That is, if  $p(t)$  denotes the overhead airslap at the site, then the near-surface particle velocity waveform,  $U(t)$ , associated with reverberation of the airslap-induced pulse in a surficial layer of thickness  $H$  can be approximated by series:

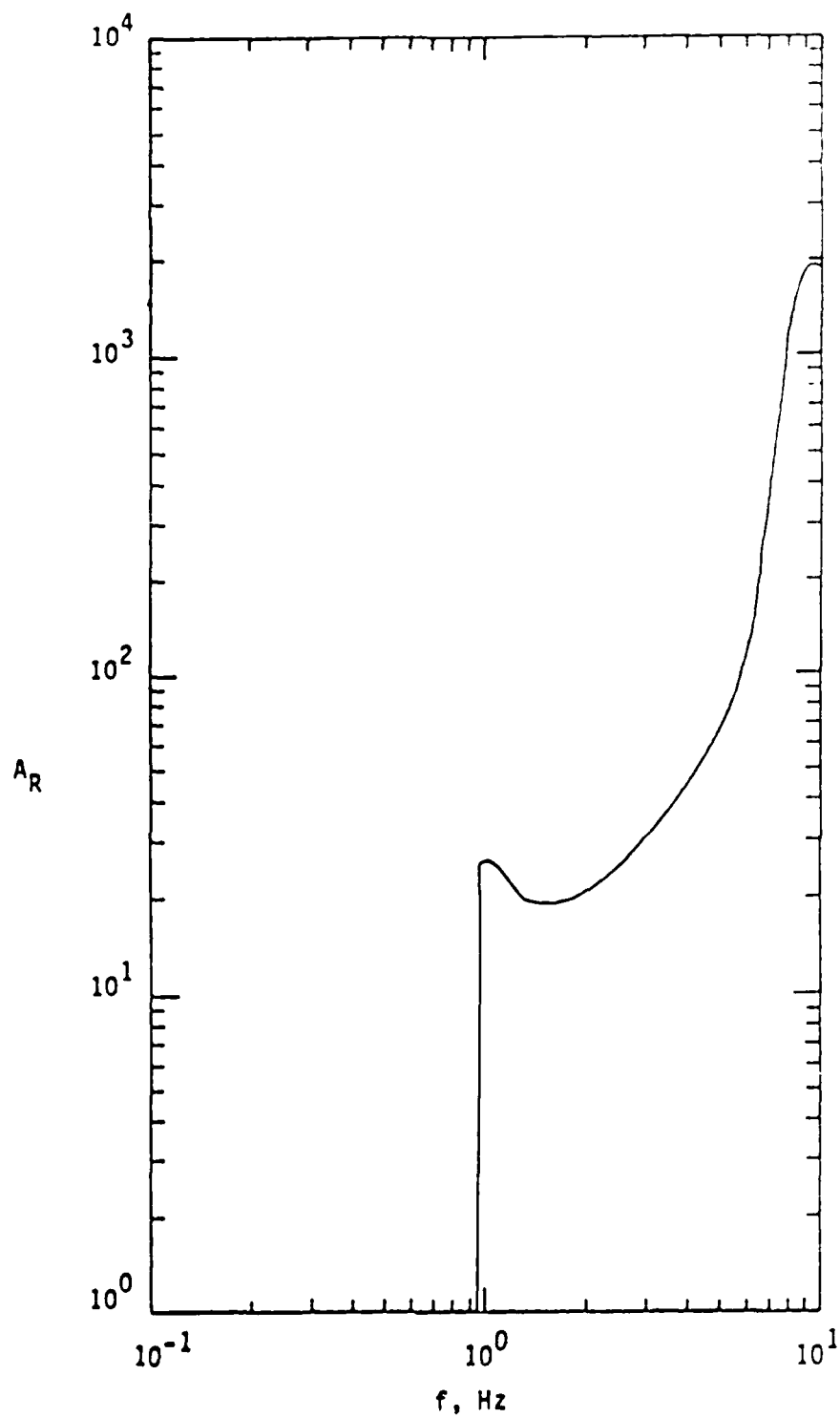


Figure 3. Fundamental mode Rayleigh wave site response function for Frenchman Flat model.

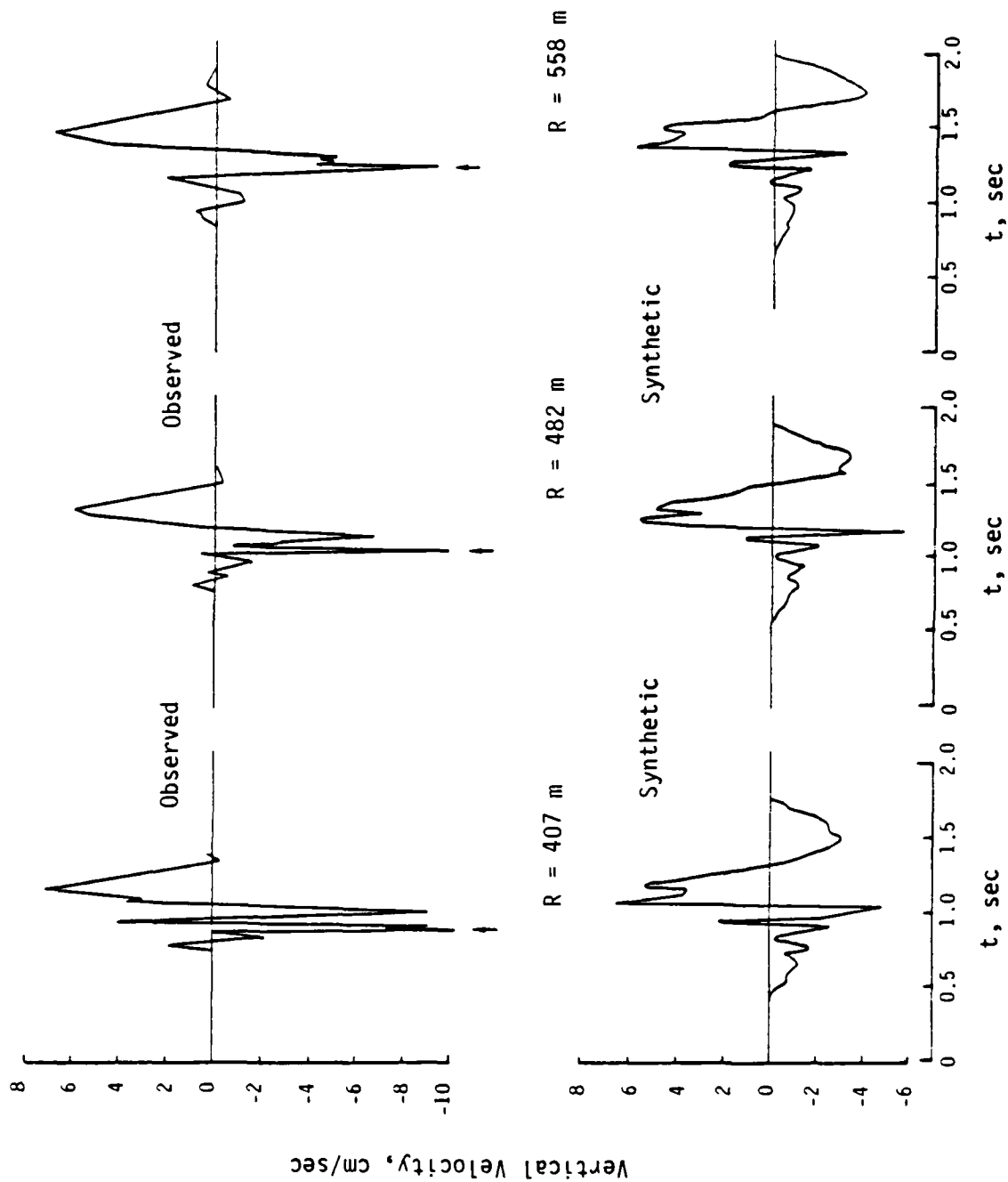


Figure 4. Comparison of observed (top) and synthetic (bottom) particle velocity waveforms for TUMBLER I. Vertical arrows denote predicted arrival times.

$$\dot{U}(t) = - \frac{p(t)}{\rho_1 \alpha_1} + 2\xi \frac{p(t - \frac{2H}{\alpha_1})}{\rho_1 \alpha_1} - 2\xi^2 \frac{p(t - \frac{4H}{\alpha_1})}{\rho_1 \alpha_1} + \dots \quad (2)$$

where  $\xi$  is the compressional wave reflection coefficient given by

$$\xi = \frac{\rho_2 \alpha_2 - \rho_1 \alpha_1}{\rho_2 \alpha_2 + \rho_1 \alpha_1} \quad (3)$$

The relative contributions of the predicted airslap-induced and Rayleigh wave components at the 482 m station are shown in Figure 5 where they are compared with the observed data. It can be concluded on the basis of this comparison that the linear superposition of these two components can account for virtually all the significant observed motion from TUMBLER I at these ranges.

There remains, however, one minor, puzzling aspect of the comparisons shown in Figure 4, namely that the synthetics consistently underestimate the amplitude of the observed principal velocity pulses by a small amount. Although this discrepancy is well within the normal data scatter, it is surprising in that the synthetics have been computed assuming a perfectly elastic response and this should provide a conservative upper bound to the observations, at least on the average. Thus, the observed discrepancy suggests the possibility that other, unaccounted for arrivals may be making noticeable contributions to the observed motion. In order to test this hypothesis, the contribution of the first higher mode Rayleigh wave has been computed and compared to that of the fundamental. Figure 6 shows such a comparison of the computed fundamental and first higher mode contributions for the 407 m station together with the result of superposing of the two components. It can be seen that the higher mode waveform is more impulsive than that associated with the fundamental and contributes significantly to the superposition only in a narrow arrival time window centered at about 1 second. Moreover, comparing the synthetic superposed waveform of Figure 6 with the waveform observed at that range from Figure 4, it can be seen that the first higher mode contribution introduces a high frequency character which is not evident in the observed signal. However, it may be that the incorporation of some

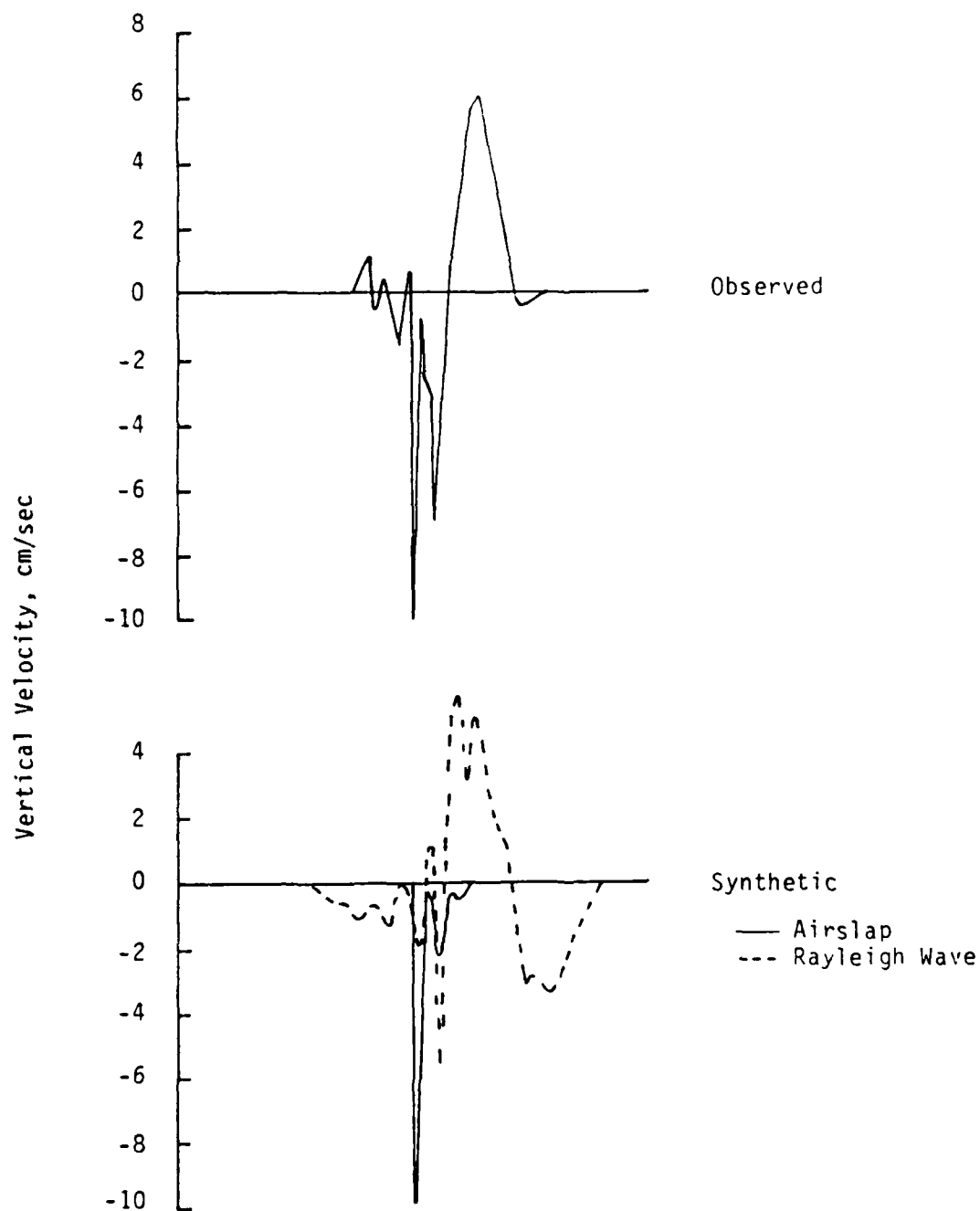


Figure 5. Comparison of observed (top) with synthetic (bottom) airlap-induced and Rayleigh wave vertical particle velocity waveforms for TUMBLER I,  $R = 482$  m.

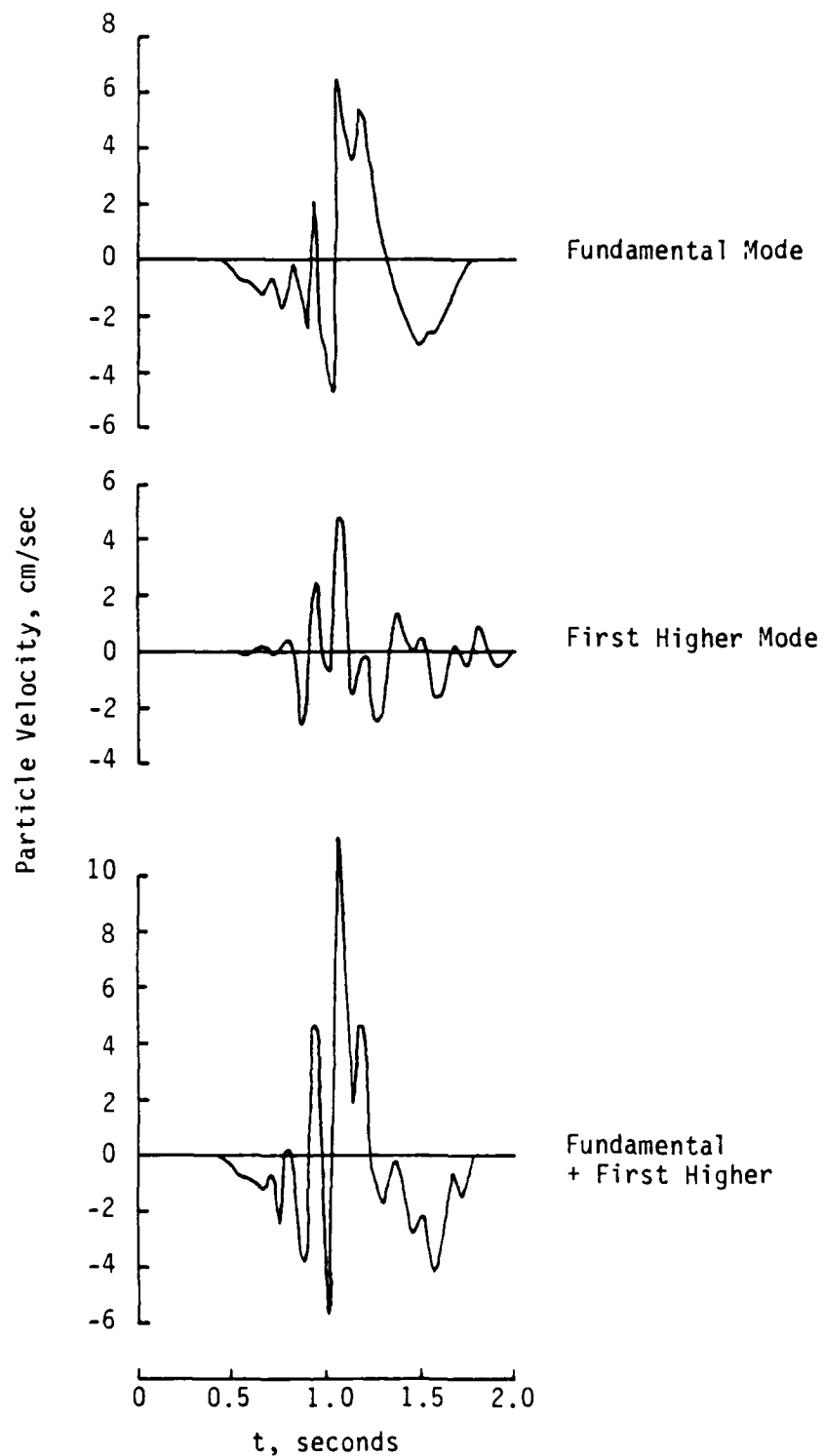


Figure 6. Comparison of fundamental and first higher mode Rayleigh wave contributions to vertical particle velocity waveforms for TUMBLER I, R = 407 m.

realistic anelastic attenuation, in conjunction with the addition of the higher mode contribution, might provide a somewhat better fit to the observations. In any case, the evidence seems to indicate that the higher mode contributions are relatively minor in this case.

#### 2.2.2 UPSHOT-KNOTHOLE 10.

This test, with its scaled HOB of about  $65 \text{ m/kt}^{1/3}$ , is intermediate between the TUMBLER I and the near-surface SMALL BOY explosions, and is unusual in that it was fired from an artillery piece (cf. Table 1). Ground motion data from this test have been processed and published by Stubbs (1977) and the vertical particle velocity waveforms recorded at five stations in the horizontal distance range extending from about 100 to 1000 m are reproduced in Figure 7. It can be seen that the data are of variable quality, but that all exhibit some long period drift which makes it difficult to resolve and analyze the lower frequency, oscillatory components of the recorded ground motion. This is a common problem with much of the available ground motion data from atmospheric nuclear explosions. Although the signals of Figure 7 have been digitized, no filtering other than a simple baseline adjustment has been applied, so as to preserve the data in its original state. While this is a commendable approach from a documentation standpoint, it seems clear that the utility of such data for purposes of ground motion analysis could be greatly increased through the application of suitable highpass filters. Unfortunately, the digital data corresponding to the waveforms in Figure 7 are not readily accessible at the present time. However, for purposes of illustration, these published waveforms have been hand-digitized and filtered using a simple, second-order highpass filter with a corner frequency of 0.5 Hz. This filter effectively eliminates spectral components with periods longer than about 2 seconds, thereby improving the resolution of the transient ground motions. This is illustrated in Figures 8-12 which show comparisons of the unfiltered and filtered waveforms for the five stations of Figure 7. As expected, these filtered versions provide a clearer representation of the oscillatory, low frequency motions of interest in the present investigation. Of course, these results need to be treated as preliminary in that

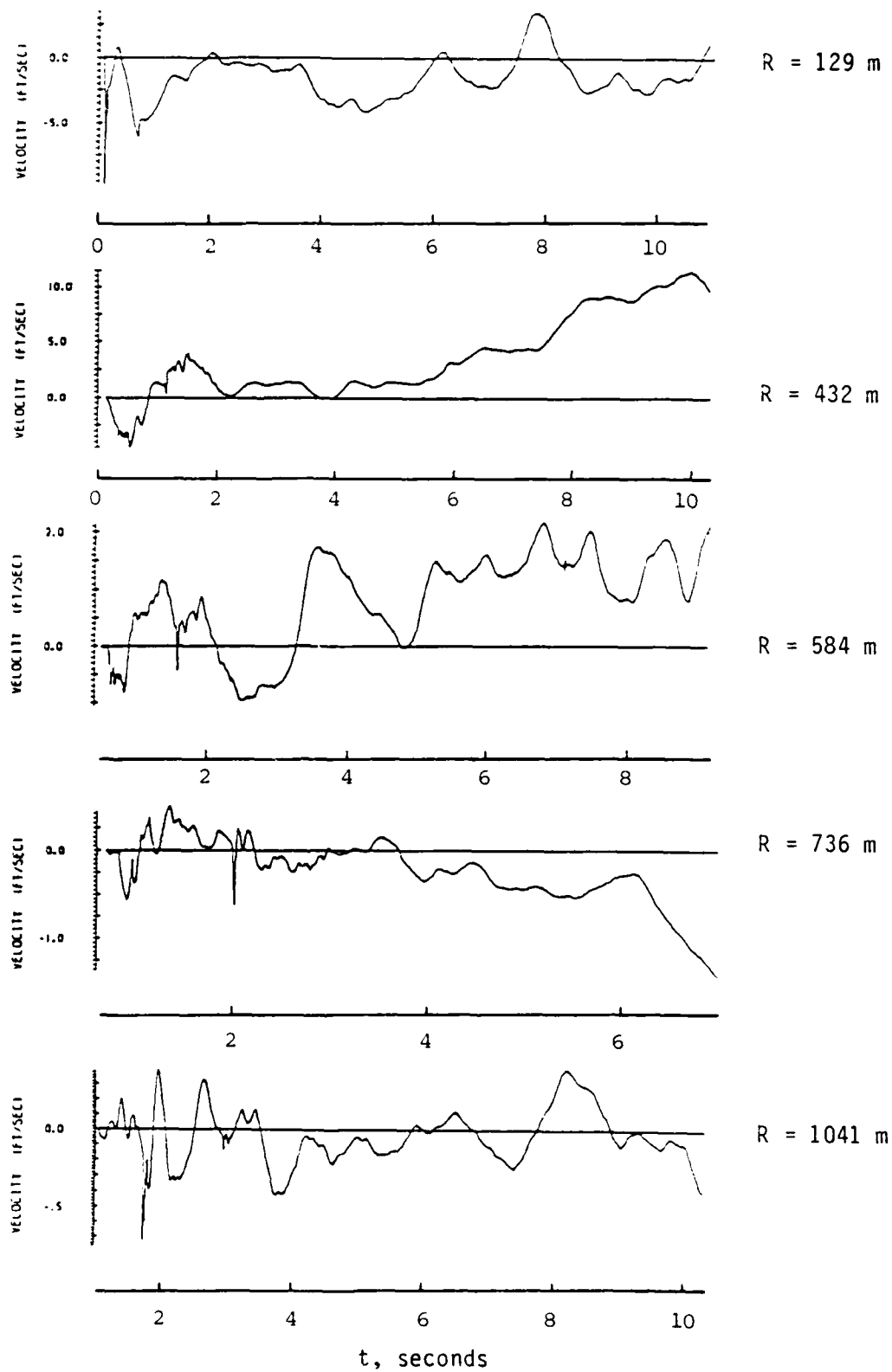


Figure 7. Vertical particle velocity waveforms for UPSHOT-KNOTHOLE 10.

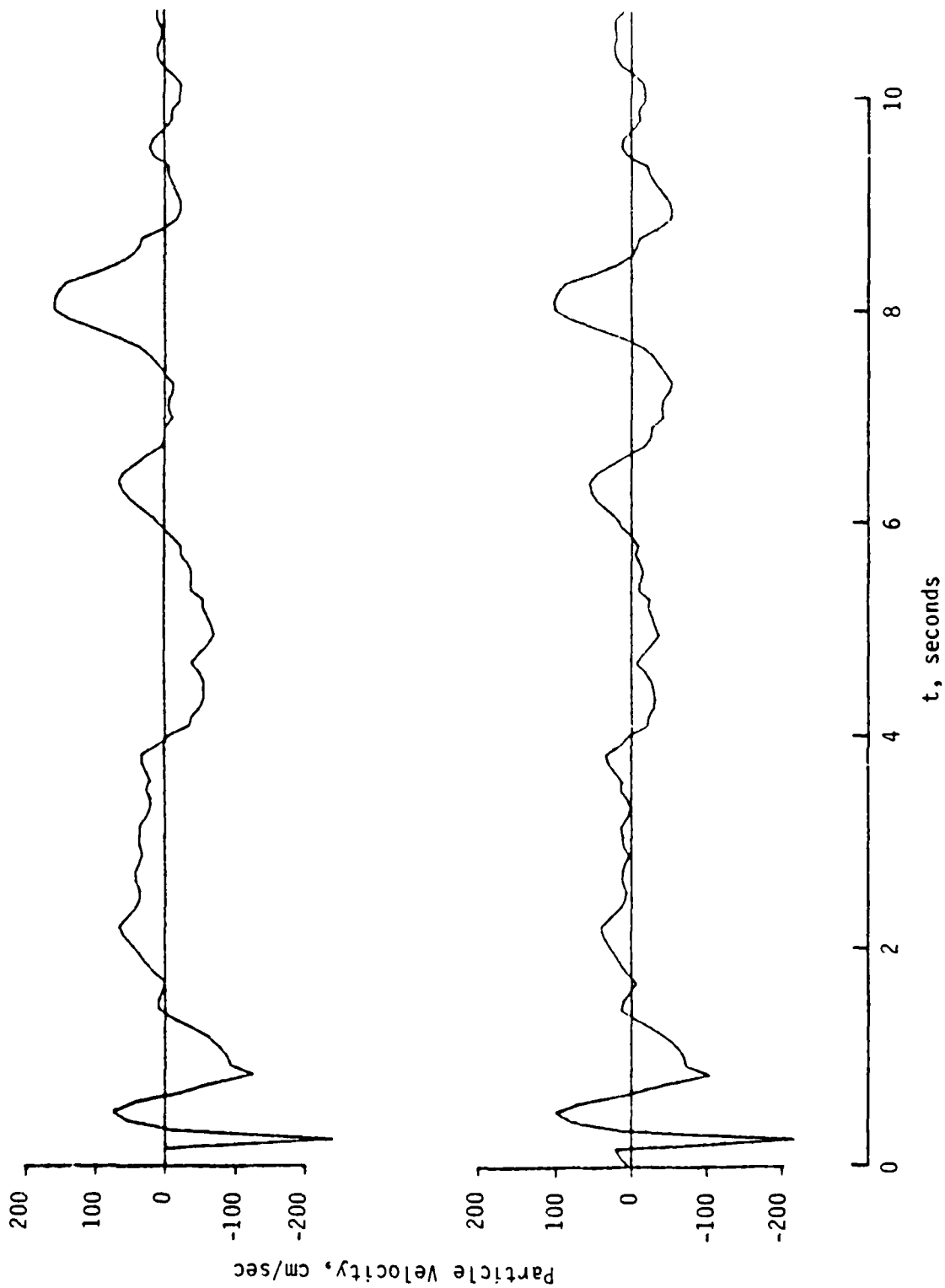


Figure 8. Comparison of unfiltered (top) and filtered (bottom) vertical particle velocity waveforms for UPSHOT-KNOTHOLE 10,  $R = 129$  m.

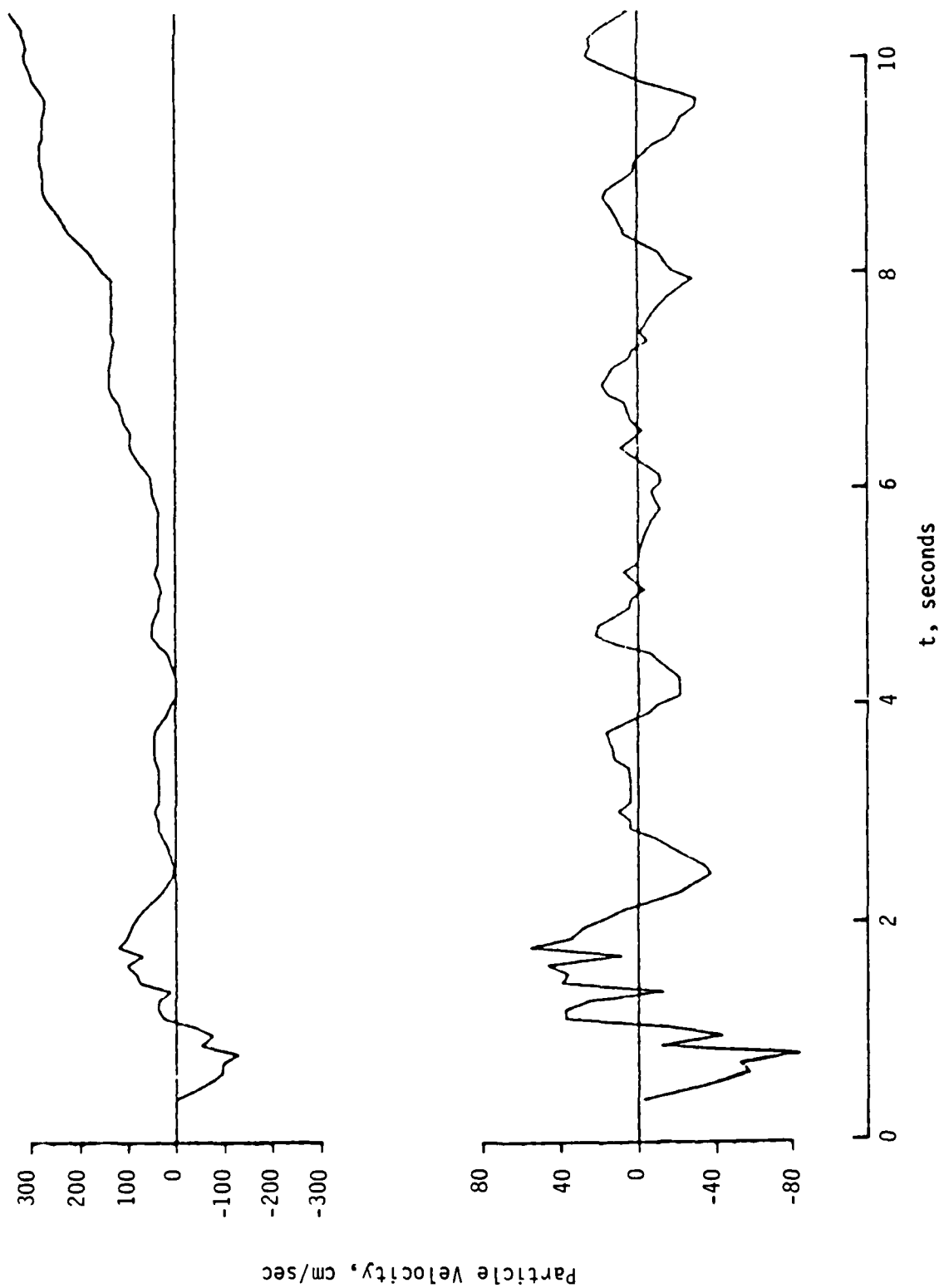


Figure 9. Comparison of unfiltered (top) and filtered (bottom) vertical particle velocity waveforms for UPSHOT-KNOTHOLE 10,  $R = 432$  m.

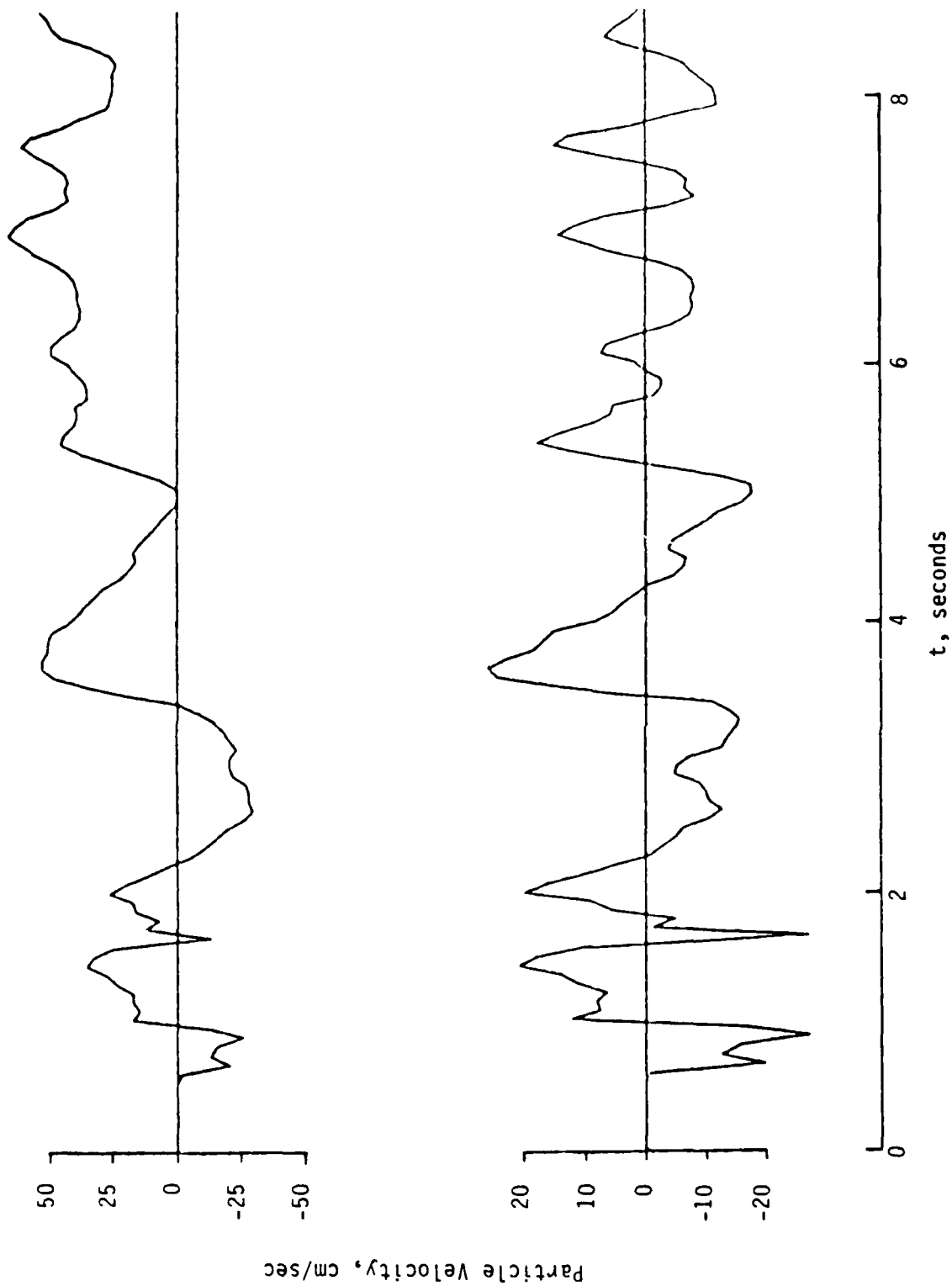


Figure 10. Comparison of unfiltered (top) and filtered (bottom) vertical particle velocity waveforms for UPSHOT-KNOTHOLE 10,  $R = 584$  m.

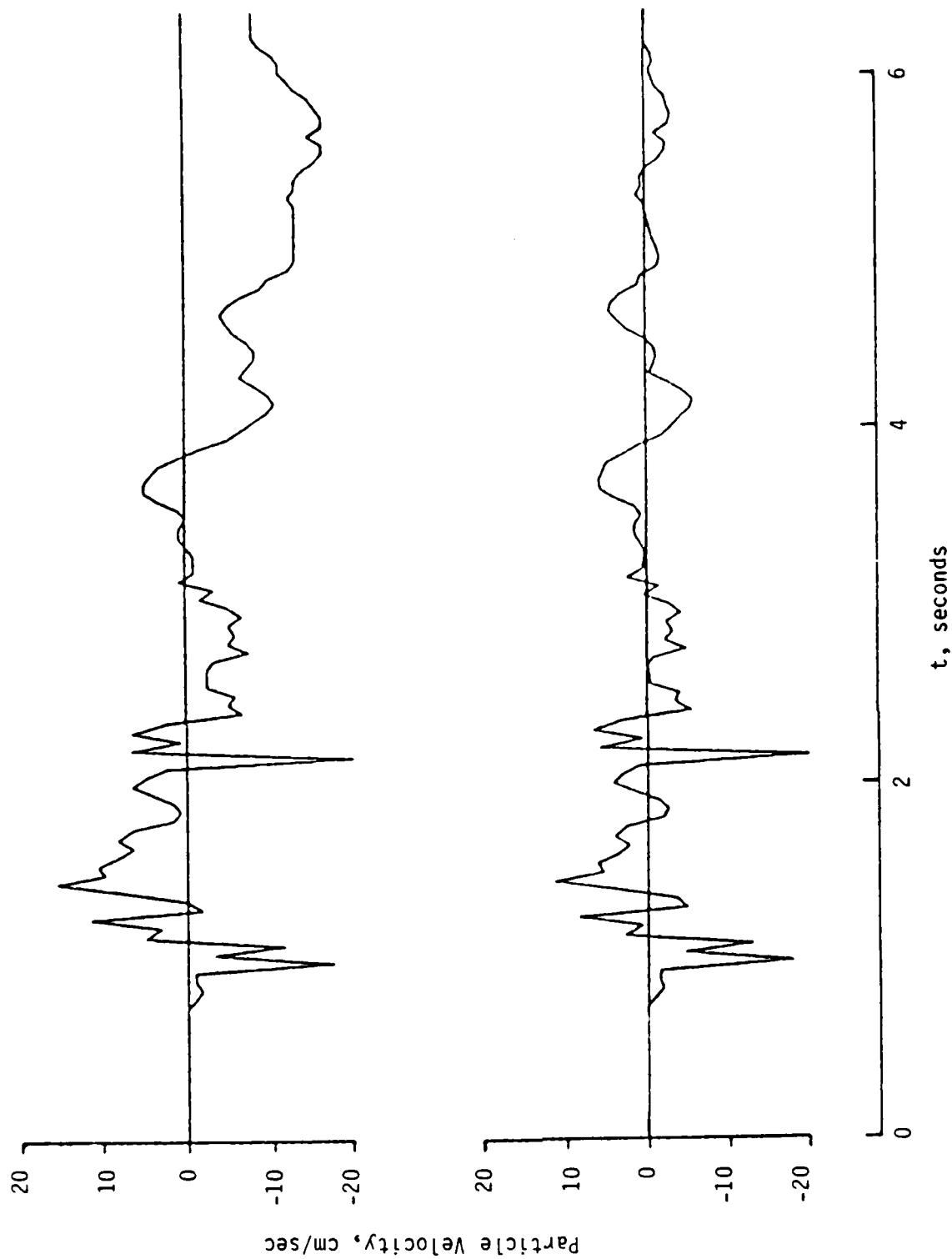


Figure 11. Comparison of unfiltered (top) and filtered (bottom) vertical particle velocity waveforms for UPSHOT-KNOTHOLE 10,  $R = 736$  m.

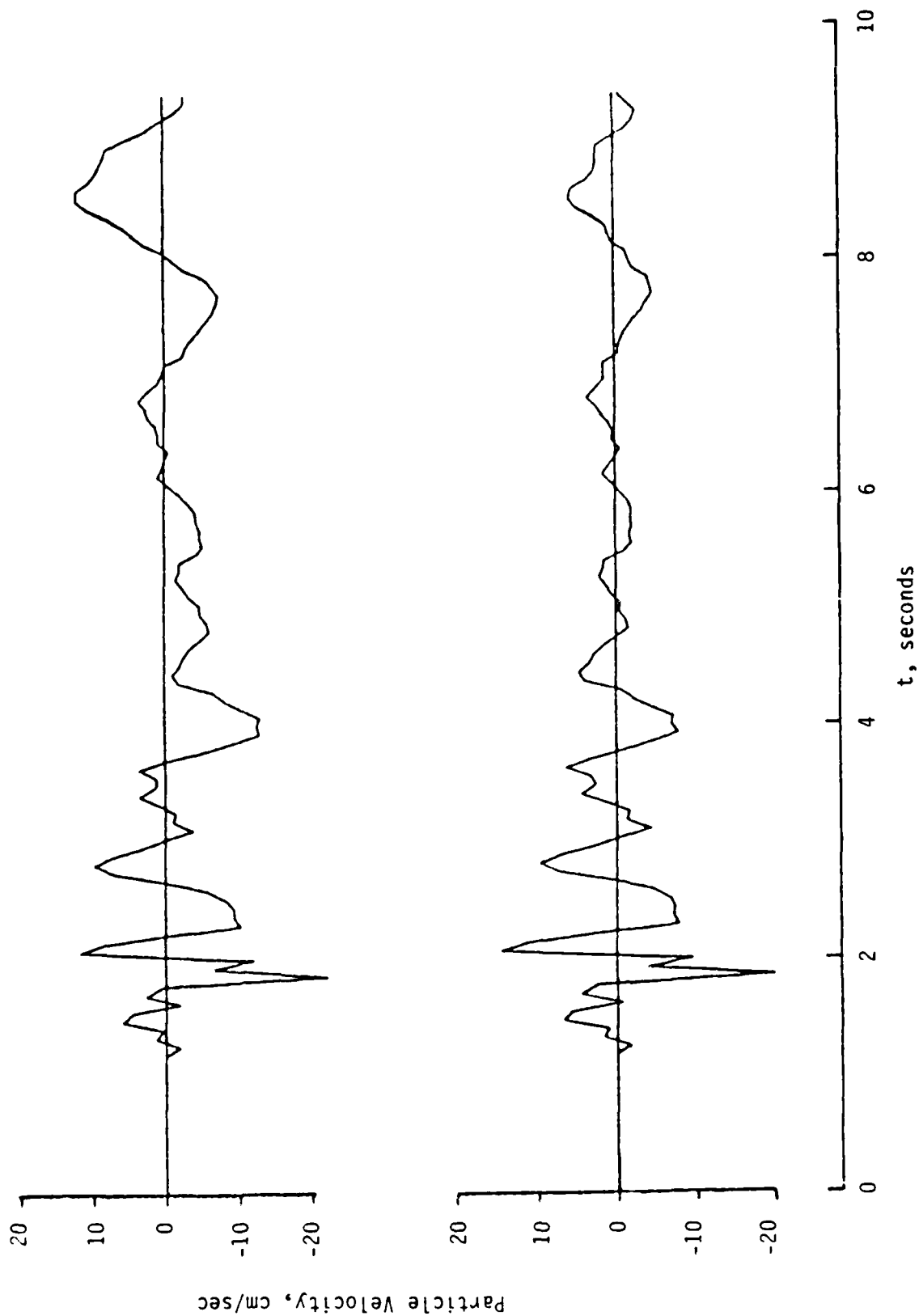


Figure 12. Comparison of unfiltered (top) and filtered (bottom) vertical particle velocity waveforms for UPSHOT-KNOTHOLE 10,  $R = 1041$  m.

the resolution which can be obtained by hand-digitizing waveforms plotted to the scale of Figure 7 is obviously quite limited. This is particularly true for the nearer stations where the motion tends to be dominated by the high-frequency, airslap-induced components. Clearly, much more reliable results are attainable if the original digitizations of Stubbs (1977) can be recovered and filtered in this manner. In the meantime, the present simulation analysis of UPSHOT-KNOTHOLE 10 will focus on the filtered velocity data for the two more distant stations (i.e.,  $R = 736$  m, 1041 m).

As with TUMBLER I, the low frequency ground motions from UPSHOT-KNOTHOLE 10 have been theoretically simulated using the Frenchman Flat geologic model of Figure 1 together with an airblast loading predicted by the Speicher and Brode (1981) analytic approximation. Again, as a first approximation,  $r_0$  in Equation (1) is assumed to be zero. Figure 13 shows the comparison between the observed and fundamental mode, synthetic vertical particle velocity waveforms for the most distant station at a range of 1041 m. It can be seen that the predicted and observed waveforms agree quite well with respect to arrival time, dominant frequency and amplitude level. However, the onset of the observed Rayleigh wave arrival is more impulsive than that of the synthetic, suggesting that other arrivals may be making a noticeable contribution in this case. This hypothesis is confirmed in Figure 14 which shows a comparison of the predicted contributions of the fundamental and first higher modes at the range of 1041 m. It can be seen that although the 1 Hz oscillatory component of the first higher mode is quite small relative to that associated with the fundamental mode, the initial impulsive motions for the two modes are of comparable magnitude. The synthetic obtained by superposing the contributions of these two modes is shown in Figure 15, where it is compared with the observed data. Comparing with Figure 13, it can be seen that the fit to the onset of the surface wave arrival has been significantly improved by the addition of the higher mode contribution. In fact, as with TUMBLER I, essentially all of the significant motion at this range, with the exception of the airslap-induced component which is identified by the vertical arrow in Figure 15, can be explained by the airblast-induced Rayleigh wave. On the other hand, the predicted oscillatory component of the motion

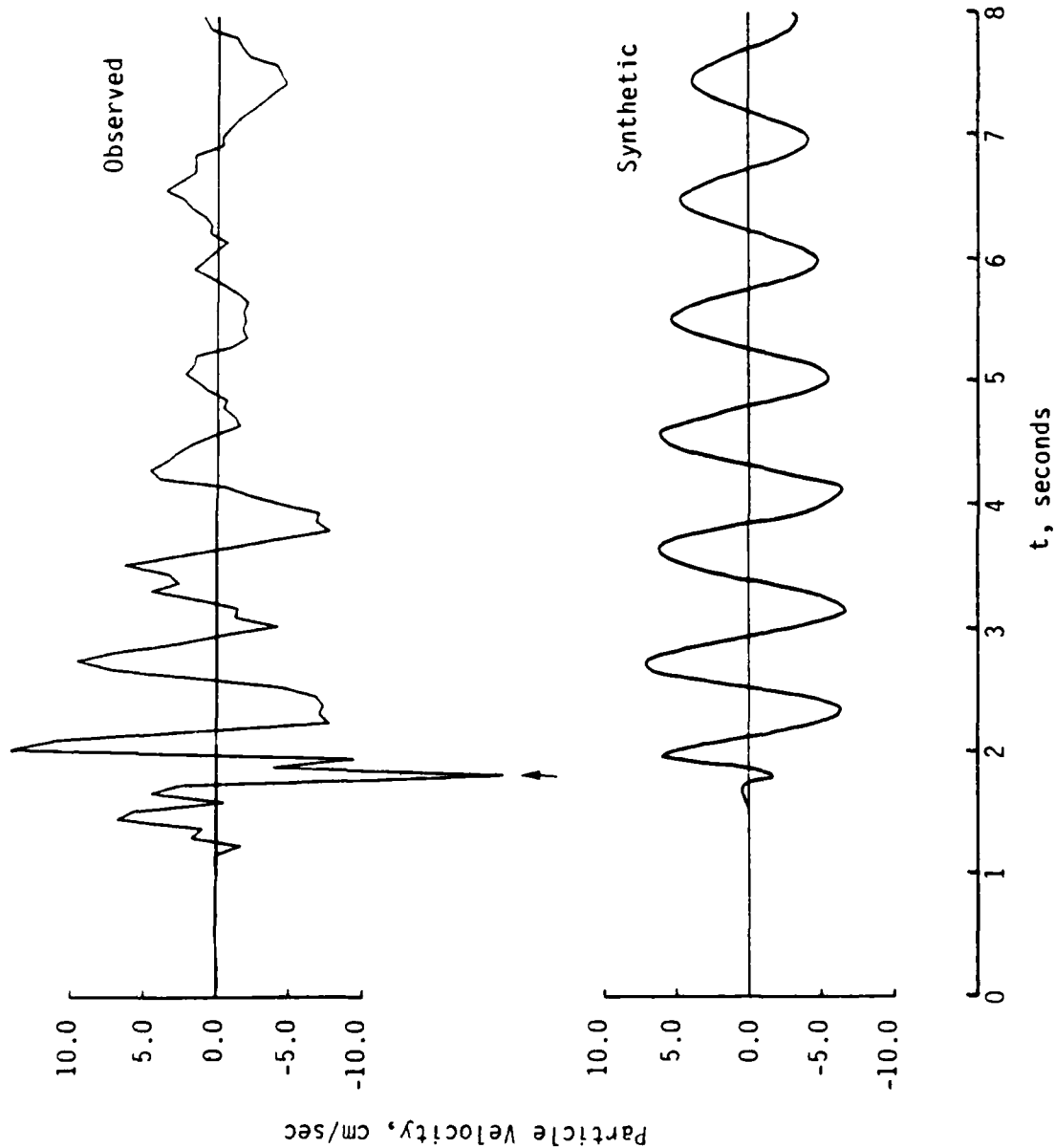


Figure 13. Comparison of observed and synthetic (fundamental mode) vertical particle velocity waveforms for UPSHOT-KNOTHOLE 10,  $R = 1041$  m. Vertical arrow denotes predicted airblast arrival time.

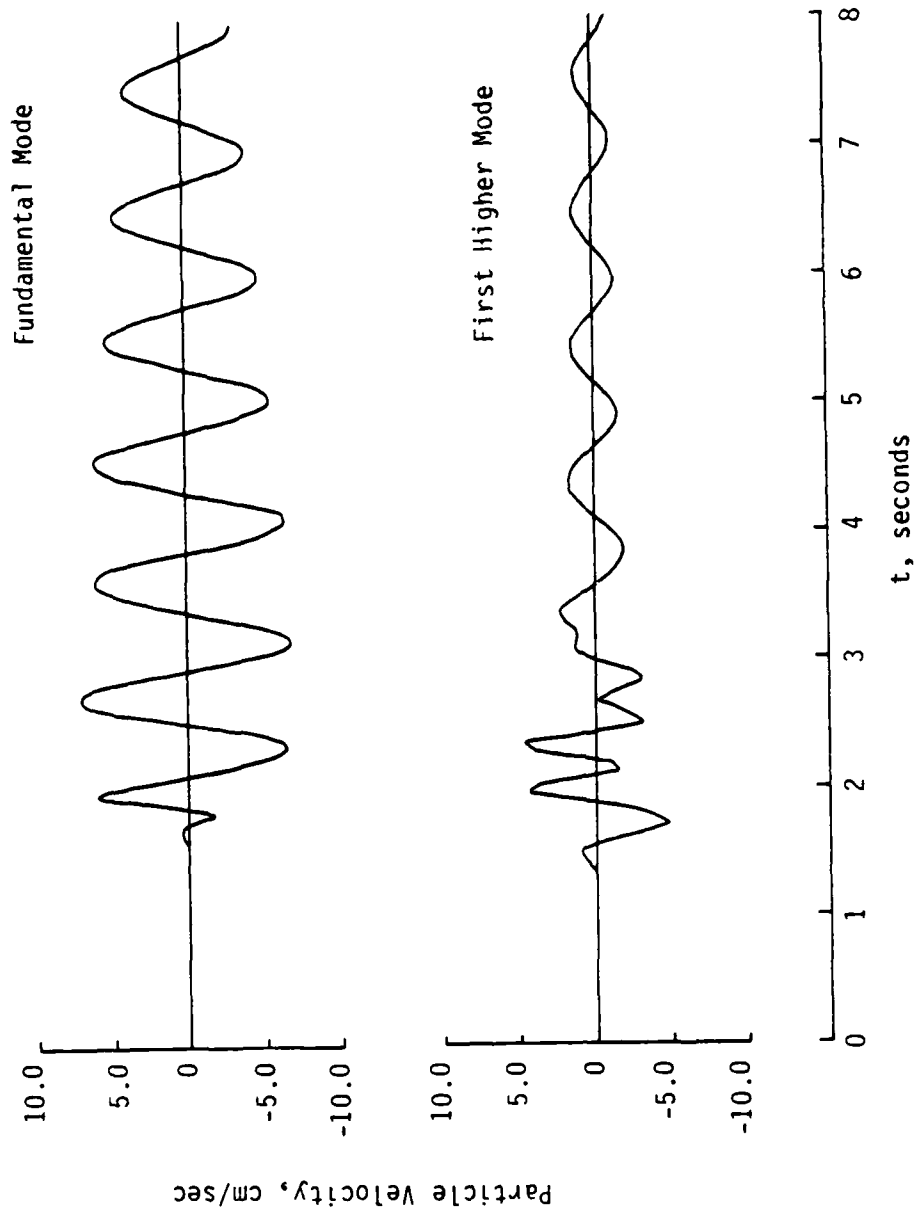


Figure 14. Comparison of fundamental and first higher mode Rayleigh wave contributions to vertical particle velocity waveforms for UPSHOT-KNOTHOLE 10, R = 1041 m.

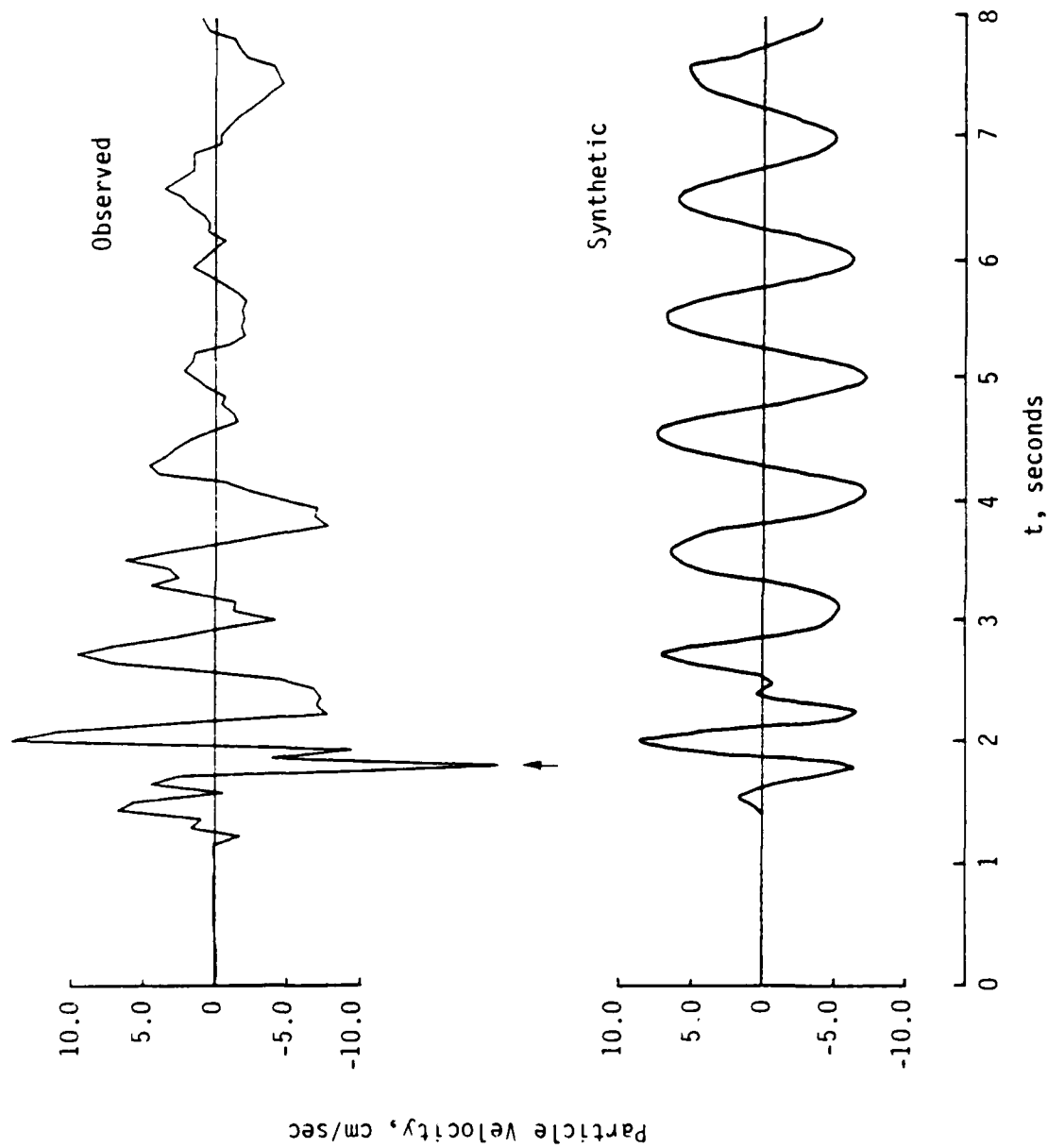


Figure 15. Comparison of observed and synthetic (fundamental plus first higher mode) vertical particle velocity waveforms for UPSHOT-KNOTHOLE 10,  $R = 1041$  m. Vertical arrow denotes the predicted airblast arrival time.

appears to have a significantly longer duration than the observed. It is not clear at this time whether this discrepancy is due to problems with the observed data at late times or whether it is a real effect, associated perhaps with scattering of Rayleigh waves by lateral heterogeneities along the propagation path. A careful re-evaluation of the original digital data may help to resolve this issue.

The comparison between the observed and synthetic (fundamental plus first higher mode) vertical particle velocity waveforms at the 736 m range is shown in Figure 16. Again, the agreement between the predicted and observed waveforms in terms of arrival time, frequency content and amplitude level is generally satisfactory. However, in this case, the observed motion is dominated by a secondary high frequency arrival which lags the predicted airblast arrival time (vertical arrow) by more than 1 second and is not associated with the Rayleigh wave. Careful examination of Figure 7 and, more particularly, the corresponding acceleration recordings, indicates that this secondary high frequency arrival can be identified on each of the five recordings. The source of this arrival has not been isolated at the present time, but one possibility is that it is associated with the firing of the 280 mm artillery piece that was used to fire the explosive to the desired height in this test. This hypothesis can presumably be tested if the location of the gun with respect to the recording stations can be recovered from the test documentation. In any case, given the questionable quality of the available data, the agreement between the observed and synthetic particle velocity waveforms at these distances from the UPSHOT-KNOTHOLE 10 test is quite reasonable and confirms the fact that much of the observed motion can be accounted for by the airblast-induced Rayleigh wave.

#### 2.2.3 SMALL BOY.

SMALL BOY was a low yield (i.e., < 20 kt) explosion detonated at a small HOB from a tower over Frenchman Flat. In this case, it seems clear that there was strong nonlinear interaction between the airblast and the surface area around ground zero and, consequently, a nonzero exclusion radius ( $r_0$ ) is required in the evaluation of Equation (1). Although this

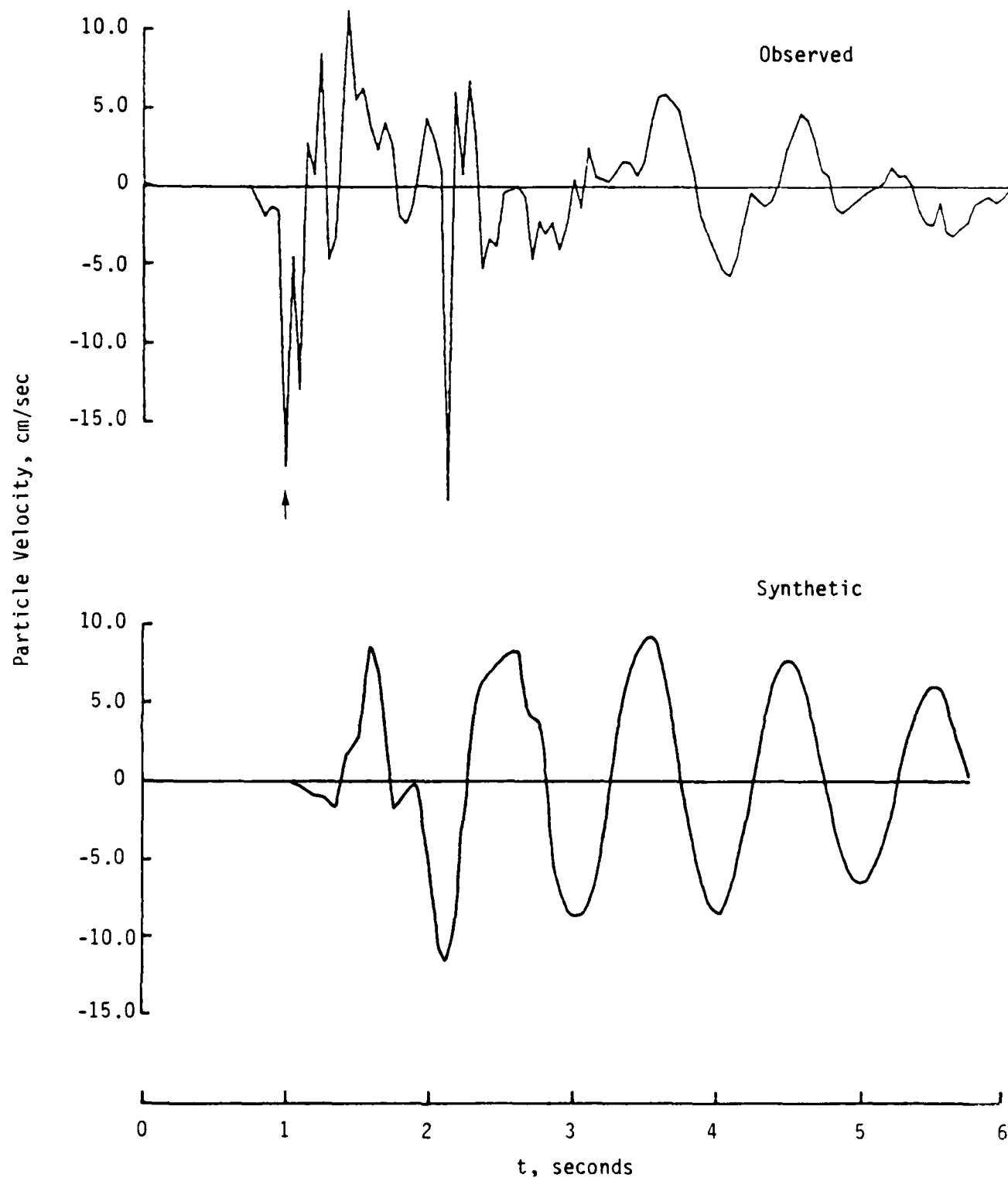


Figure 16. Comparison of observed and synthetic (fundamental plus first higher mode) vertical particle velocity waveforms for UPSHOT-KNOTHOLE 10,  $R = 736$  m. Vertical arrow denotes the predicted airblast arrival time.

radius has been found to coincide approximately with the final crater radius for HE surface bursts (Murphy, 1978), there is no available evidence to suggest how it should vary for nuclear explosions with nonzero HOB. Consequently, for simulation purposes, a preliminary exclusion radius of 30 m around ground zero has been somewhat arbitrarily adopted to define the area inside of which no airblast loading is applied. The significance of this exclusion radius with respect to low frequency ground motion simulation will be addressed experimentally later in this section.

Figure 17 shows a comparison of the observed SMALL BOY vertical displacement at a range of 2139 m with the fundamental mode synthetic computed for that range using the Frenchman Flat geologic model of Figure 1. It can be seen that the agreement is not very satisfactory. In particular, although the amplitude level is approximately correct, the group arrival time, dominant frequency and duration of motion are clearly incorrect, indicating that the subsurface model of Figure 1 is not an adequate representation of the path to this station. In fact, it is difficult to see how any strongly layered subsurface model could give rise to the observed simple displacement pulse at this relatively large range. This observation motivated an investigation into the possibility that a simple halfspace model might provide a reasonable approximation to the observed data. In particular, a halfspace model was selected which has a shear wave velocity consistent with the observed Rayleigh wave group arrival time at this station (i.e.,  $\beta = 327$  m/sec). Figure 18 shows a comparison of the vertical displacement computed using this halfspace model with the observed SMALL BOY data at a range of 2139 m. It can be seen that the agreement between theoretical and observed obtained using this model is quite good with respect to the dominant frequency, amplitude level and duration of motion. The corresponding particle velocity comparison is shown in Figure 19. Again, the agreement is very good, even including the relative arrival time and approximate amplitudes of two prominent, high frequency, secondary arrivals at around 7.0 seconds. It is somewhat puzzling that a different subsurface model is required to explain the observed ground motion from SMALL BOY, given its proximity to the other two tests (cf. Table 1). However, it was detonated near the center of the dry

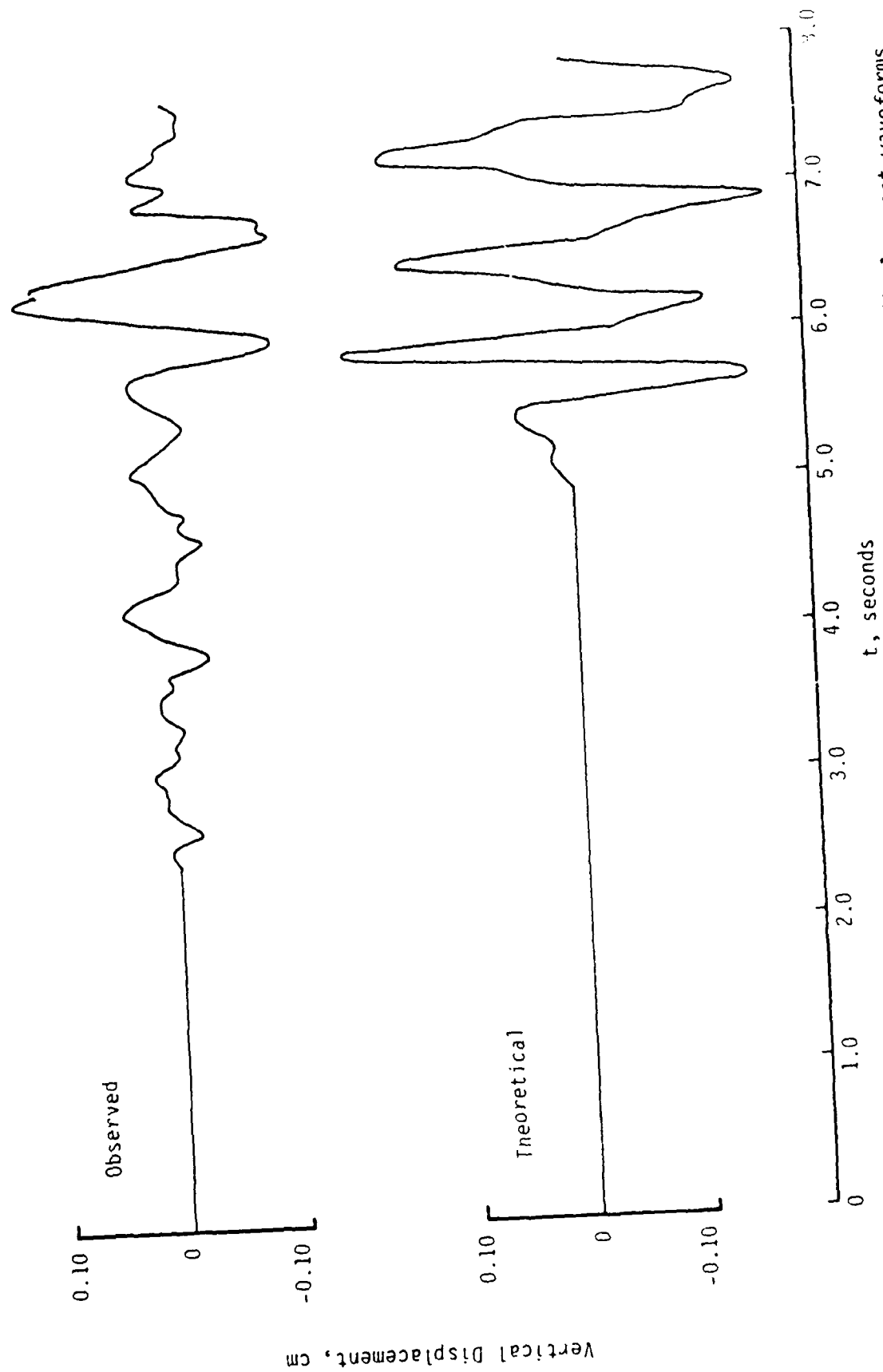


Figure 17. Comparison of observed (top) and synthetic (bottom) vertical particle displacement waveforms for SMALL BOY at a range of 2139 m, Frenchman Flat subsurface model.

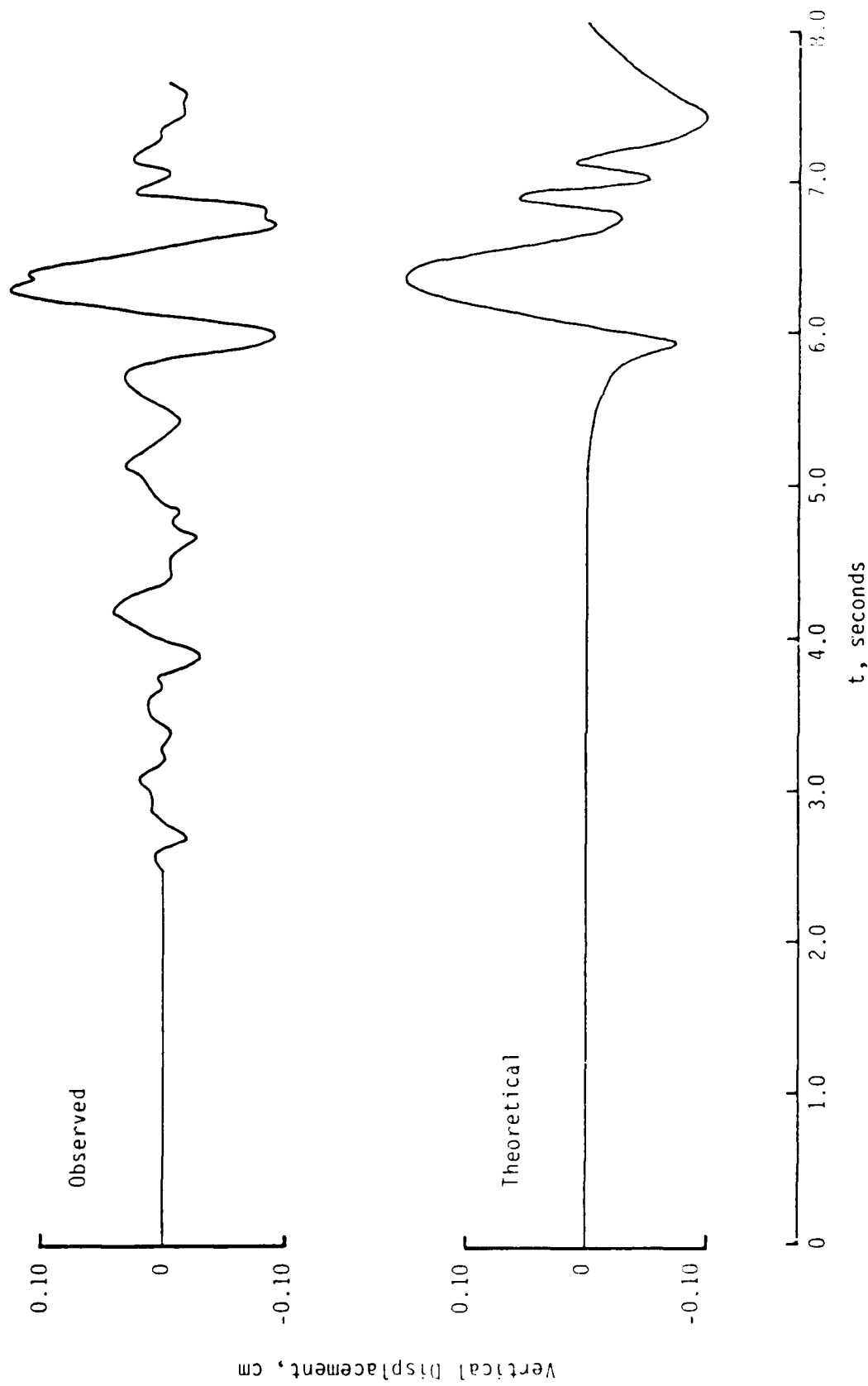


Figure 18. Comparison of observed (top) and synthetic (bottom) vertical particle displacement waveforms for SMALL BOY at a range of 2139 m, halfspace model.

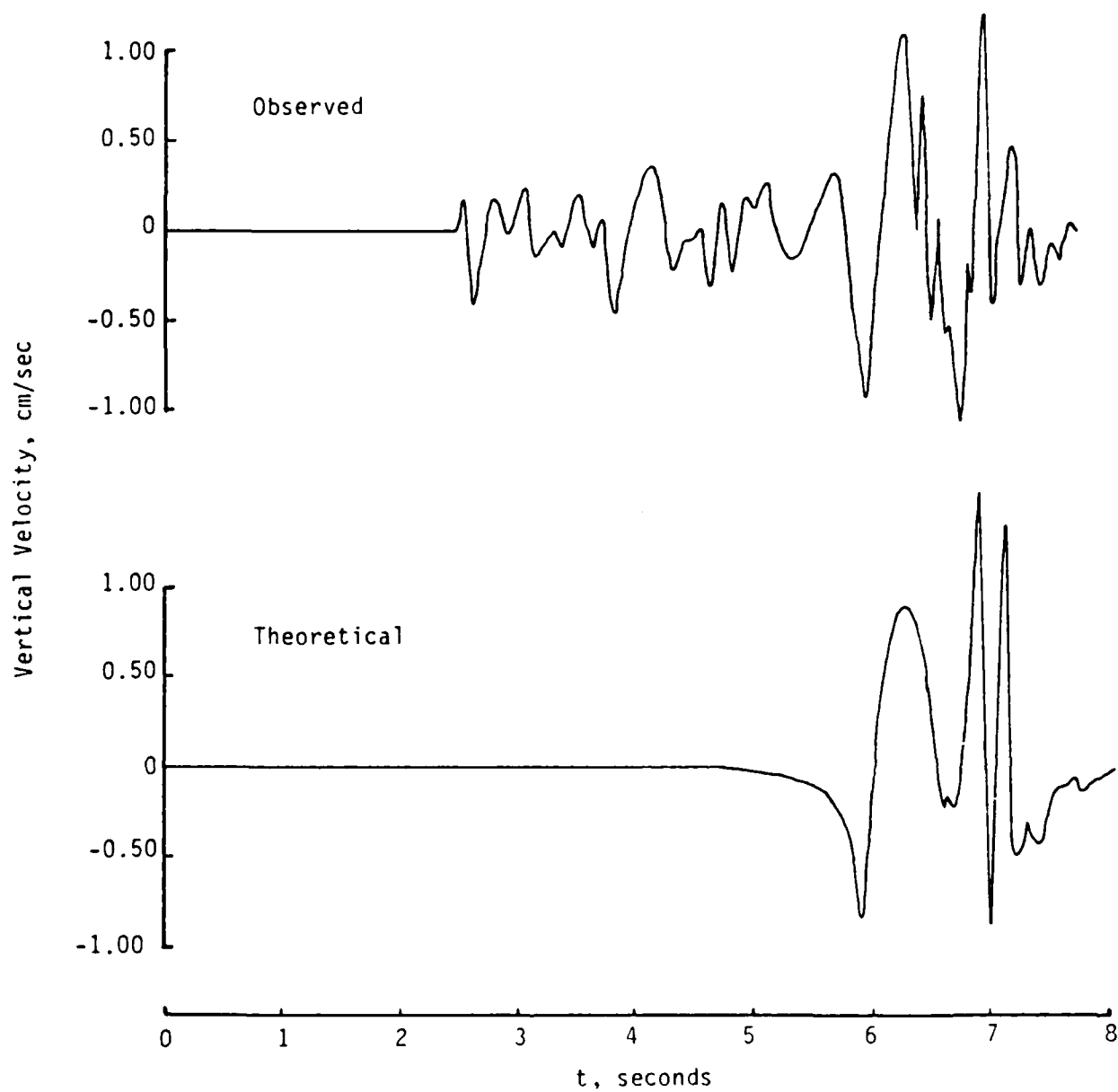


Figure 19. Comparison of observed (top) and synthetic (bottom) vertical particle velocity waveforms for SMALL BOY at a range of 2139 m, halfspace model.

lake bed and it may well be that the propagation path to this station crosses a different portion of Frenchman Flat than those characteristic of the other two tests. Unfortunately, the available documents describing the ground motion experiments on these tests do not specify the map coordinates of the stations, so it is not possible to compare the propagation paths in any detail at this time. In any case, the observed low frequency ground motions clearly indicate that such differences exist.

Returning now to the particle velocity comparison of Figure 19, it can be seen that the theoretical Rayleigh waveform is considerably more complex than that which would be expected from a point surface load on a halfspace. It follows that the propagating airblast loading must result in a complex, multi-component seismic source function. For an observation point at large distance from ground zero, the Rayleigh wave source function is given by the integral expression (Murphy and Bennett, 1980):

$$S(\omega) = \int_{r_0}^{r_{\max}} p(r', \omega) J_0(kr') r' dr' \quad (4)$$

where, for the applications shown in Figures 18 and 19,  $r_0 = 30$  m and  $r_{\max} = 1000$  m. Of course, by linearity, the integral in Equation (4) can be decomposed into a sum of integrals of the form:

$$\int_{r_0}^{r_{\max}} = \int_{r_0}^{r_1} + \int_{r_1}^{r_2} + \dots + \int_{r_n}^{r_{\max}} \quad (5)$$

and thus it is possible to evaluate the contribution of any arbitrary surface ring loading to the computed waveform. Figure 20 shows a comparison of the synthetic particle velocity waveform of Figure 19 with the individual contributions computed from the loading of an inner ring extending from 30 to 100 m and from an outer ring extending from 100 to 1000 m. Note that the two high frequency secondary arrivals at around 7.0 seconds arise from the loading of the inner ring (30-100 m), while the initial lower frequency arrival at around 6.0 seconds can be essentially completely

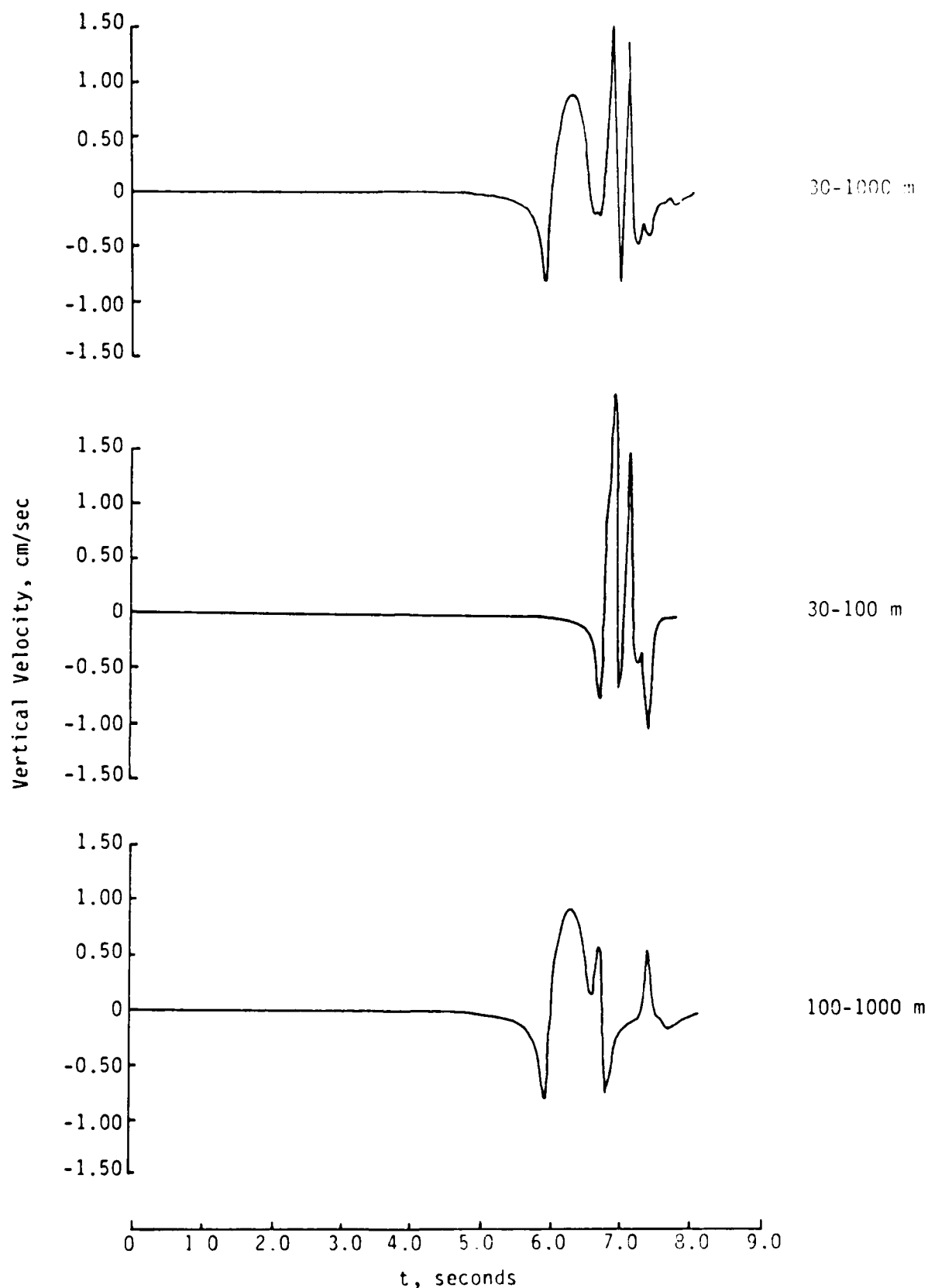


Figure 20. Comparison of composite synthetic velocity waveform (top) with contributions arising from loading of inner (30-100 m, center) and outer (100-1000 m, bottom) rings, SMALL BOY,  $R = 2139$  m.

accounted for by the contributions from the outer ring (100-1000 m). This is physically reasonable in that in the inner ring the overpressure loading is impulsive (i.e., has a short duration) and highly supersonic, while in the outer ring the positive phase duration becomes significant (with respect to the seismic frequency band of interest) and the airblast propagation velocity drops down into the seismic velocity range. Another observation that can be made with regard to Figure 20 is that there are additional high frequency pulses arriving at about 7.5 seconds on the waveforms computed from the individual ring loads which appear to have no counterpart on the composite waveform. These pulses have no physical significance and are merely an artifact of the truncation of the loading at 100 m. This sudden truncation introduces a negative pulse from the inner ring and an equal and opposite positive pulse from the outer ring which cancel out in the composite, as required by the physics of the problem.

The decomposition of the loading shown in Figure 20 also provides insight into the significance of the exclusion radius,  $r_0$ . That is, a reduction in  $r_0$  can be expected to increase the high frequency components of the induced ground motion without significantly affecting the low frequency components. This inference is confirmed in Figure 21 which shows a comparison of the observed particle velocity waveforms from Figure 19 with the synthetics computed assuming  $r_0$  values of 30 and 20 m respectively. As expected, the only significant change in the synthetics is in the relative amplitude of the high frequency secondary arrivals. In fact, this comparison confirms that the initial value of 30 m is about right and that smaller values of  $r_0$  lead to poorer agreement with the observations. If anything, a slightly larger value of  $r_0$  is suggested by these data. In fact, nearly exact agreement can be obtained by tapering the onset of loading at 30 m rather than turning it on discontinuously. For example, Figure 22 shows a comparison of the observed particle velocity data with the synthetic computed by linearly tapering the applied overpressure in the 30 to 60 m range. These examples confirm that the exclusion radius concept is a reasonable approximation which is remarkably consistent with these observations.

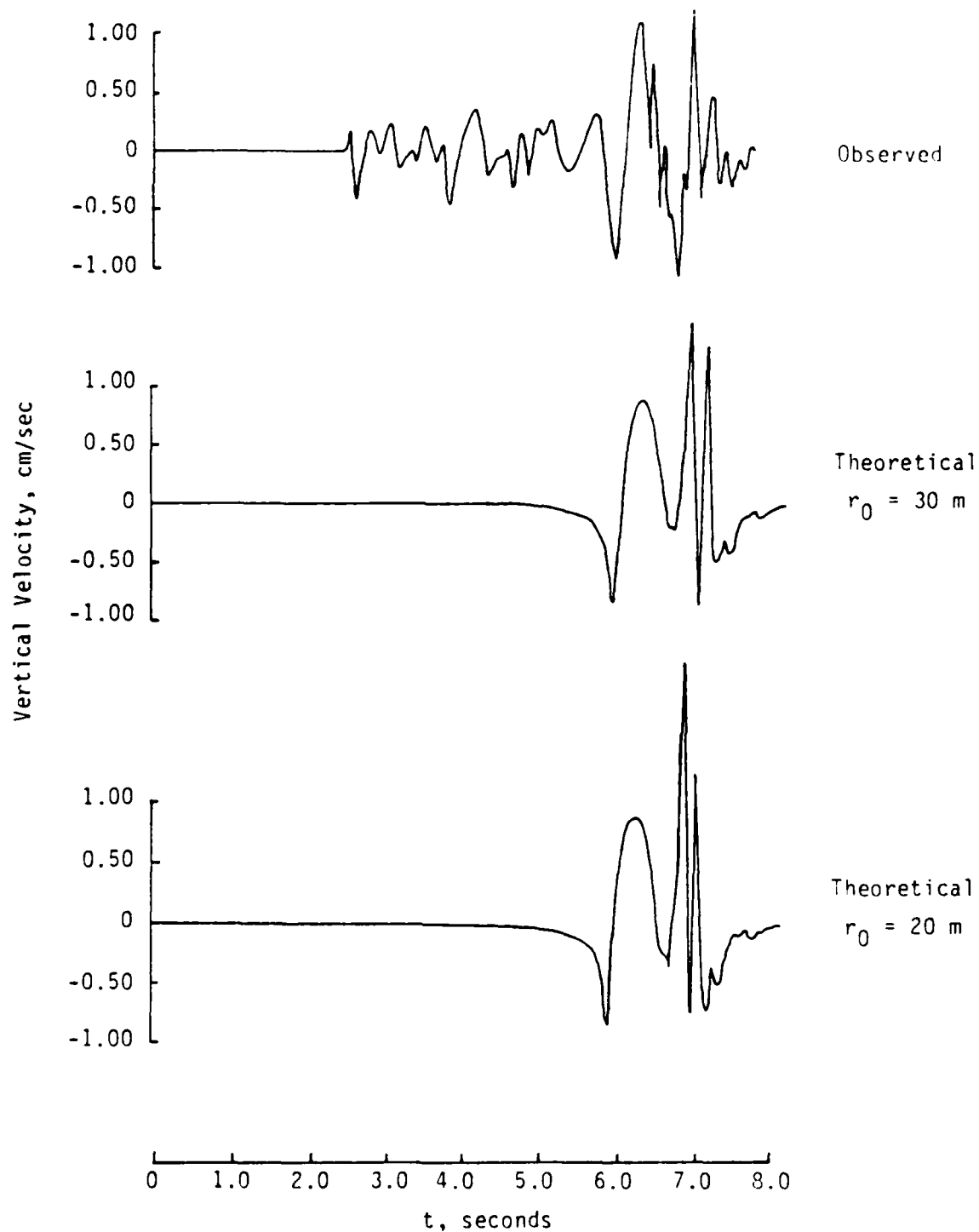


Figure 21. Comparison of observed vertical particle velocity waveform with synthetics computed using different values of the exclusion radius ( $r_0$ ), SMALL BOY,  $R = 2139 \text{ m}$ .

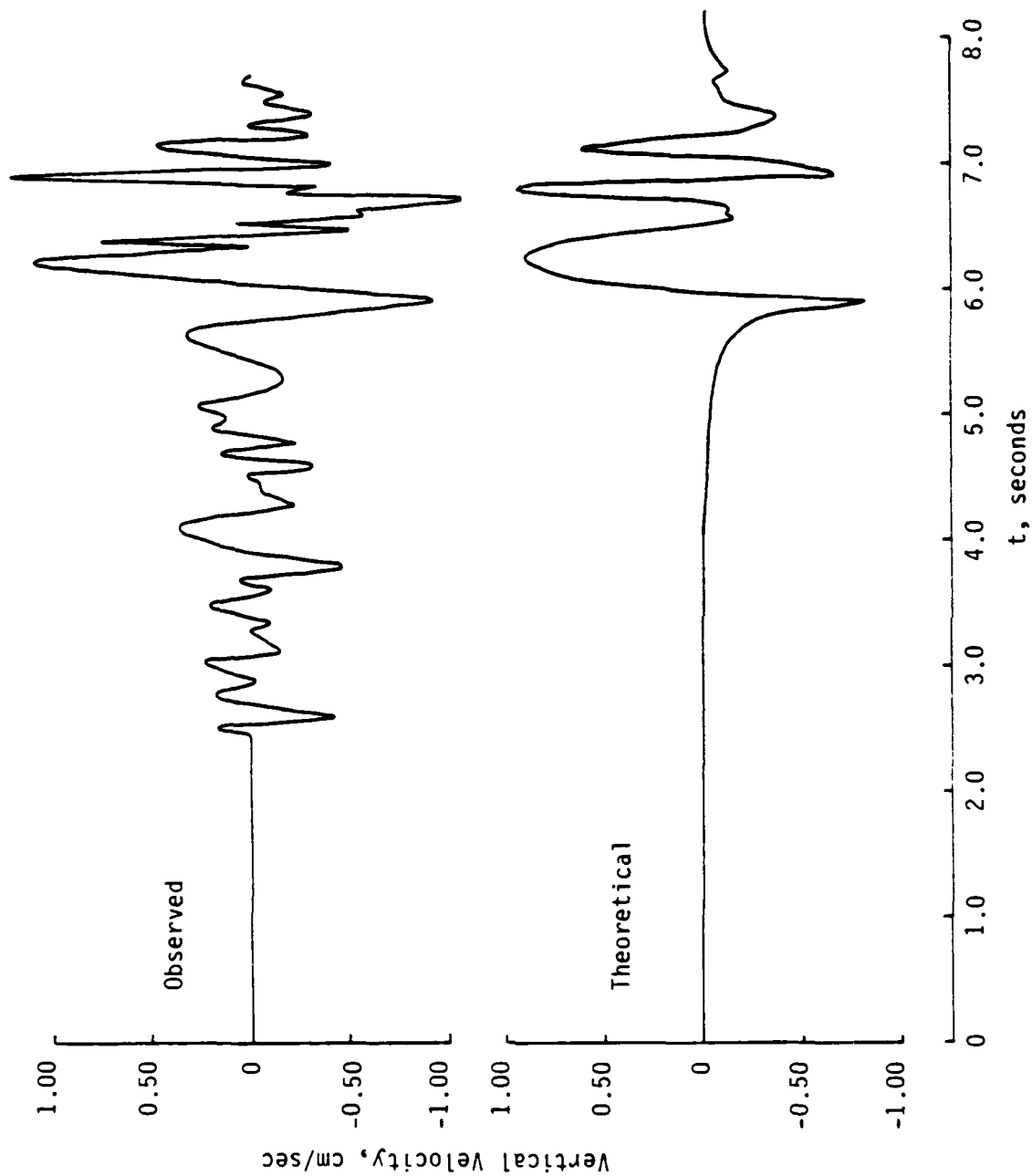


Figure 22. Comparison of observed (top) and synthetic (bottom) vertical particle velocity waveforms for SMALL BOY at a range of 2139 m, halfspace model, linear tapering of the overpressure between 30 and 60 m.

## SECTION 3

### PREDICTION AND SCALING CONSIDERATIONS

#### 3.1 BACKGROUND.

The results presented in Section II of this report have confirmed the fact that the low frequency ground motions observed from selected atmospheric nuclear tests at NTS can be largely accounted for by the airblast-induced elastic surface waves. This validation under full scale nuclear conditions represents a significant advance over the previous analyses of HE data. However, as in the HE studies, the simulation analyses of these nuclear events were "post-dictions" of data which had been recorded many years before and, thus, not directly applicable to the assessment of prediction capability. Therefore, in the next section, an example of some recent experience with the actual prediction of the Pre-DIRECT COURSE experiment low frequency ground motions will be presented to illustrate some of the aspects of the prediction process. This will be followed by an outline of some of the basic scaling relations which are implied by the model and which can be used in the preliminary evaluation of the effects of site geology, yield, distance and instrument depth on the predicted low frequency components of the ground motion.

#### 3.2 Pre-DIRECT COURSE PREDICTIONS.

This experiment, which was conducted at the White Sands testing area in New Mexico in September, 1982 consisted of 24 tons of HE (ANFO) detonated at an HOB of about 17 m. Preliminary determinations of subsurface physical properties at the site were made on the basis of a P wave refraction survey (Personal Communication, Bob Reinke, AFWL, 1982) and are shown schematically in Figure 23 together with the corresponding predicted fundamental mode Rayleigh wave dispersion curves. It should be noted that the shear wave velocities, which control the Rayleigh wave characteristics, have not been measured at this site and, consequently, were estimated on the basis of results obtained from other sites in this general area. It can be seen that the refraction survey indicates the presence of a thick (75 m) layer of dry alluvium overlying saturated alluvium which apparently

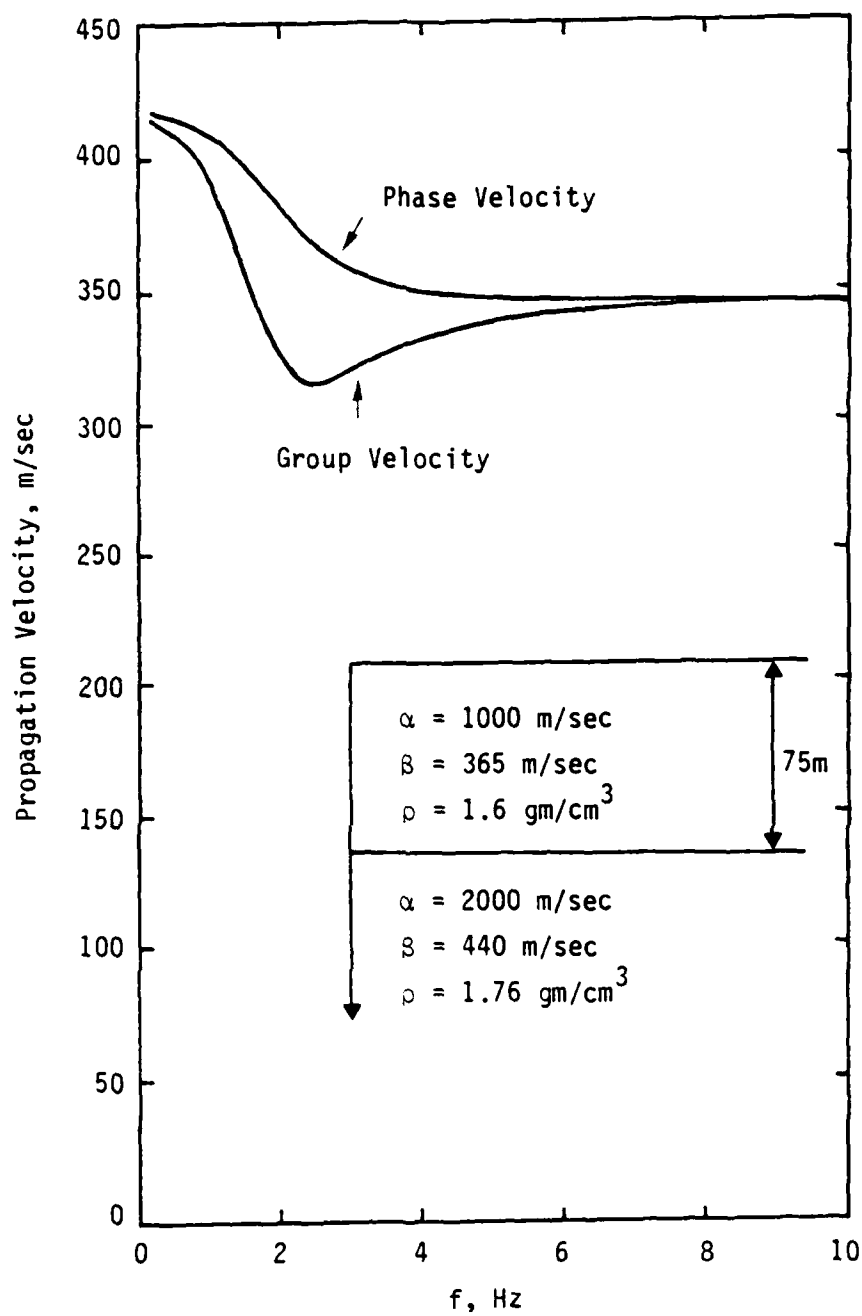


Figure 23. Subsurface geologic model and associated fundamental mode Rayleigh wave dispersion curves, Pre-DIRECT COURSE.

extends to a depth of more than 150 m (i.e., the approximate limit of resolution of the 500 m long refraction line). Note that because of the small inferred variation of shear wave velocity ( $\beta$ ) with depth, very strong dispersion of the surface wave energy is not expected at this site. However, the model does predict a distinct group velocity minimum at a frequency of about 2.5 Hz (i.e.,  $\beta_1/2H$ ). As expected, this corresponds to a pronounced corner frequency on the corresponding Rayleigh wave site response function,  $A_R(\omega)$ , shown in Figure 24. Thus, for this site model, the predominant energy in the surface wave components of the ground motion should be confined to frequencies above 2.5 Hz.

The low frequency ground motions to be expected from this test have been estimated using an airblast loading function computed from the Speicher and Brode (1981) analytic approximation for nuclear explosions, with an effective yield of 48 tons. Available evidence suggests that a nuclear explosion of this yield will produce an airblast loading essentially equivalent to that expected from the detonation of 24 tons of ANFO at that same height (Personal Communication, George Ullrich, DNA, 1982). However, in the case of Pre-DIRECT COURSE this clearly provides only a rough approximation to the loading in that the mass of the container was about 12 percent of the total explosion mass and this significantly perturbed the airblast characteristics in the high overpressure regime.

Figure 25 shows a comparison of the observed Pre-DIRECT COURSE vertical displacements at ranges of 94, 156 and 313 m with the displacements predicted theoretically using the geologic model of Figure 23 together with the airblast loading approximation described above. It can be seen that while the predicted and observed amplitude levels agree quite well, the predicted dominant frequency is too low and the predicted arrival time is consistently late. This suggests that the geologic model of Figure 23 is not an accurate representation of the actual subsurface conditions at this site. Consequently, the approximate scaling law  $f = \beta_1/2H$  (Murphy and Bennett, 1980) has been used to infer a model which is more consistent with the observed ground motion characteristics. The final model is compared with the original model in Figure 26 where it can be seen that the principal change has been to decrease the average

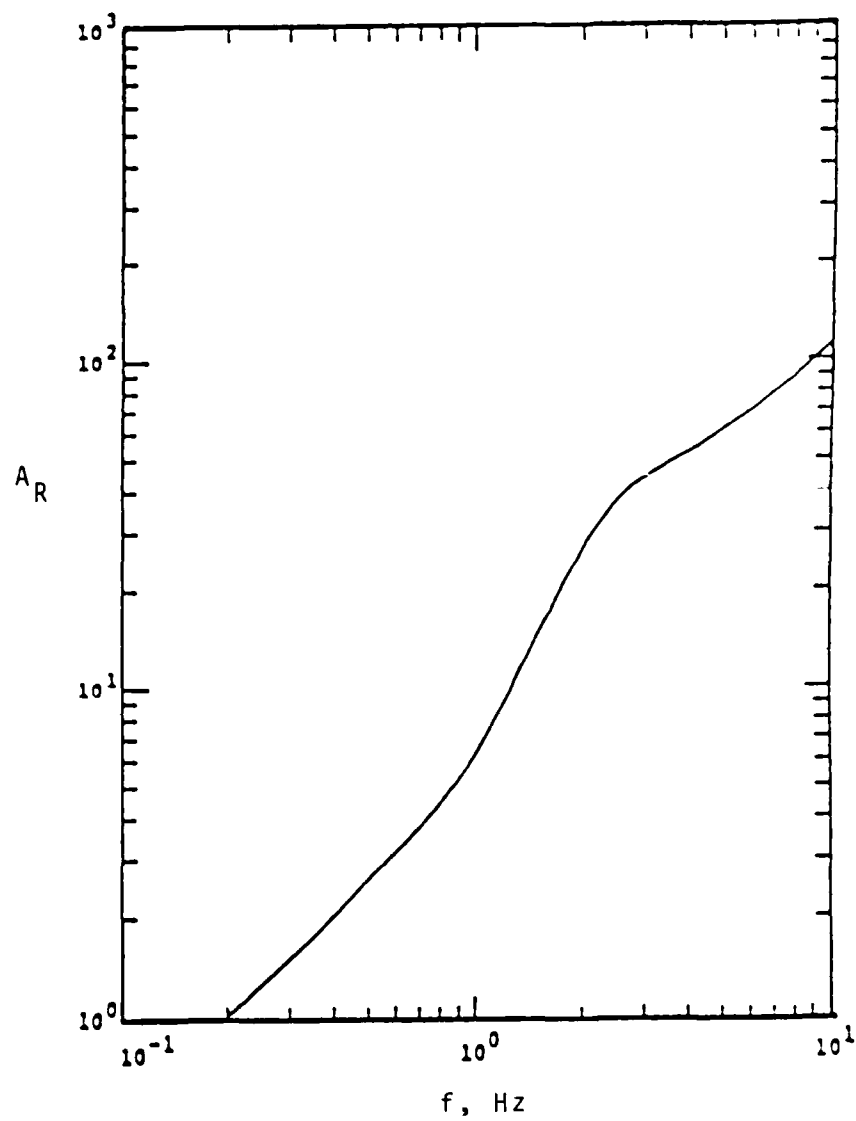


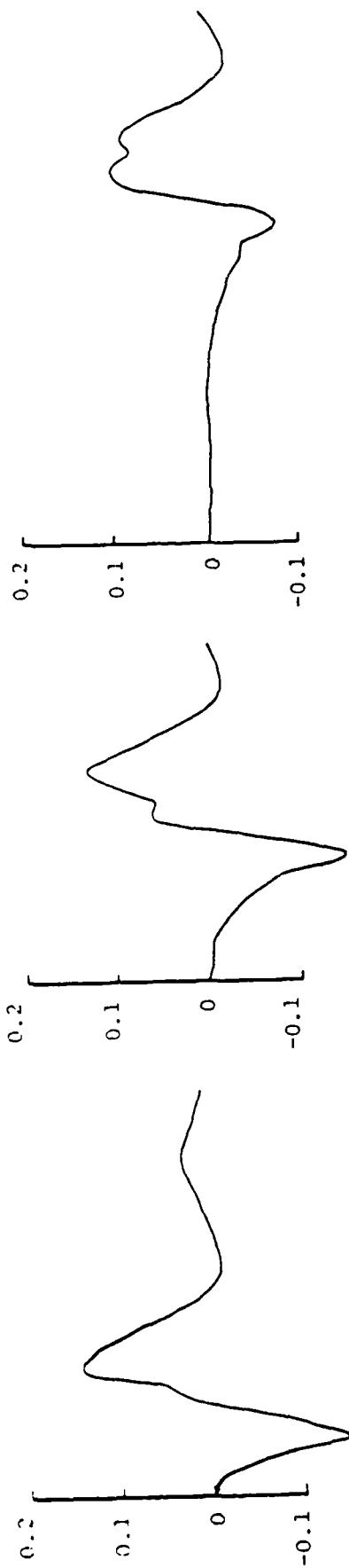
Figure 24. Pre-DIRECT COURSE Rayleigh wave site response function ( $A_R$ ).

$R = 313 \text{ m}$

$R = 156 \text{ m}$

$R = 94 \text{ m}$

Theory



Observed

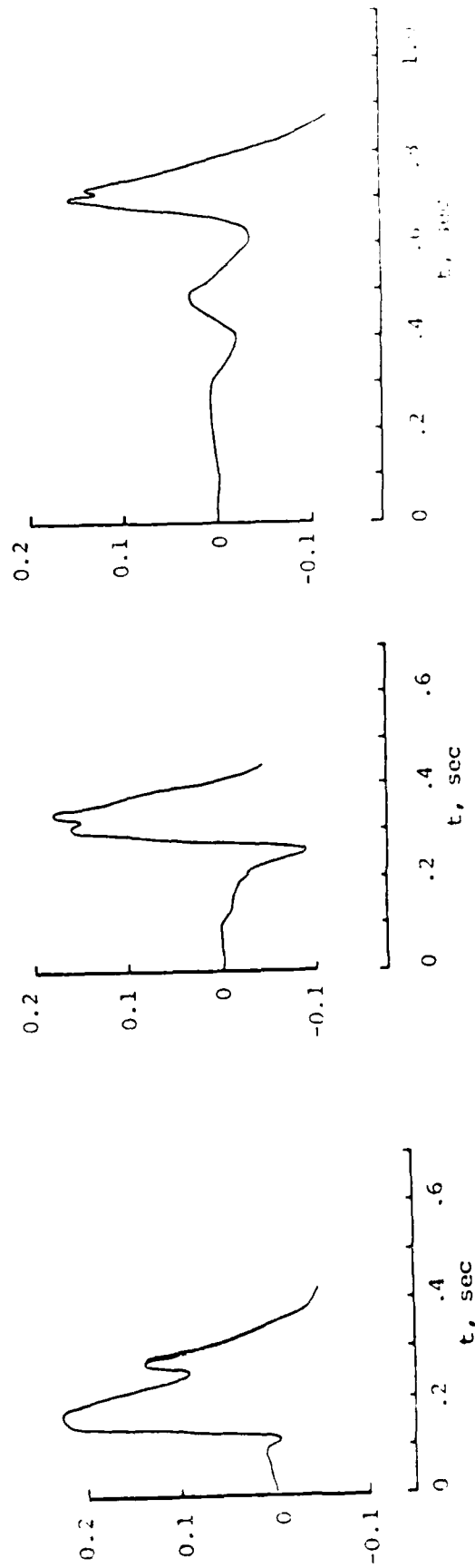
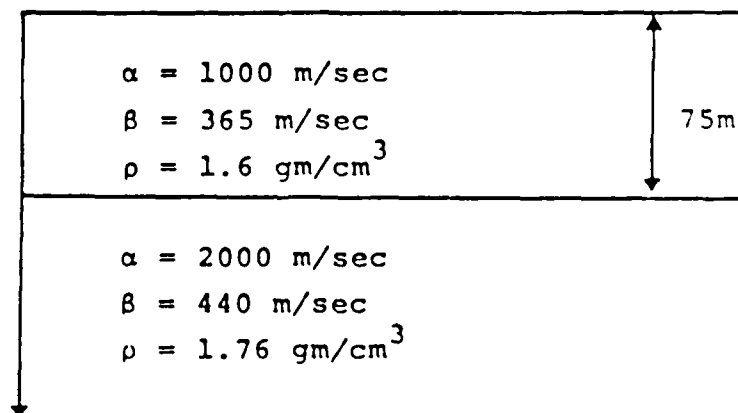


Figure 25. Comparison of predicted (top) and observed (bottom) vertical displacement waveforms for Pre-DIRECT COURSE, original site model.

### Original Model



### Final Model

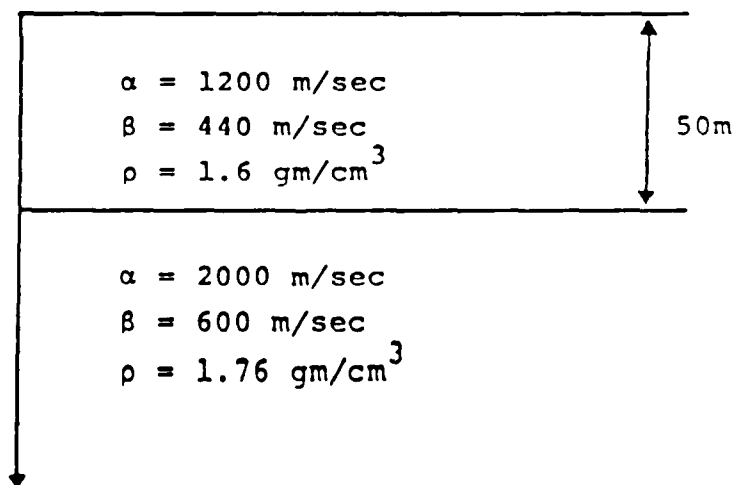


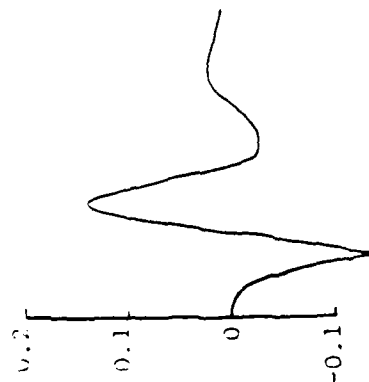
Figure 26. Comparison of original and final subsurface models for Pre-DIRECT COURSE.

surficial layer thickness from 75 m to 50 m. The theoretical displacements predicted using this final geologic model are compared with the observed data in Figure 27. It can be seen that the agreement is now well within the variability in the experimental data. Moreover, subsequent detailed geophysical surveys at the site revealed that the actual surficial layer thickness is indeed about 50 m as opposed to the original estimate of 75 m (Personal Communication, George Ullrich, DNA, 1983). Thus, the evidence provided by this experiment suggests that given an accurate model of the subsurface site geology, it should be possible to accurately predict the characteristics of the low frequency ground motions expected from atmospheric explosions. However, the predicted ground motion characteristics are clearly quite sensitive to the near-surface shear wave velocity structure, and the Pre-DIRECT COURSE experience indicates that this cannot be adequately constrained on the basis of P wave refraction surveys. Another conclusion that can be drawn from this analysis is that departures of the close-in airblast loading from the ideal represented by the Speicher/Brode analytic approximation, such as those which occurred on Pre-DIRECT COURSE, do not have a pronounced effect on the observed low frequency ground motions. That is, as has been noted previously (Murphy et al., 1982), these ground motion components are relatively insensitive to the high frequency details of the airblast.

### 3.3 SCALING CONSIDERATIONS.

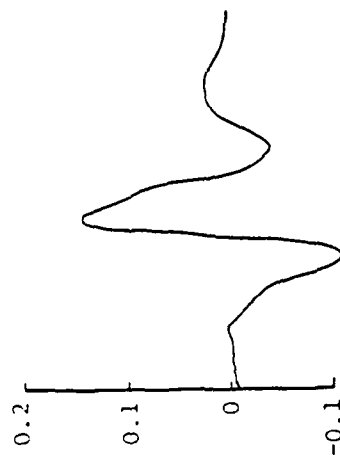
The results presented above and in the previous section indicate that it is possible to accurately estimate the complete waveforms associated with the low frequency components of the ground motions induced by atmospheric explosions, given the yield and HOB of the explosion and an accurate description of the subsurface site geology. However, in many applications in which the ground motion vulnerabilities of various strategic structures are being parametrically evaluated in a preliminary fashion, such detailed predictions are not required and what is needed are simplified scaling laws, such as those provided in EM-1. At the present time, work is still in progress on the development of a simple, theoretically-based scaling model which can be used to approximate all the low frequency

R = 94 m

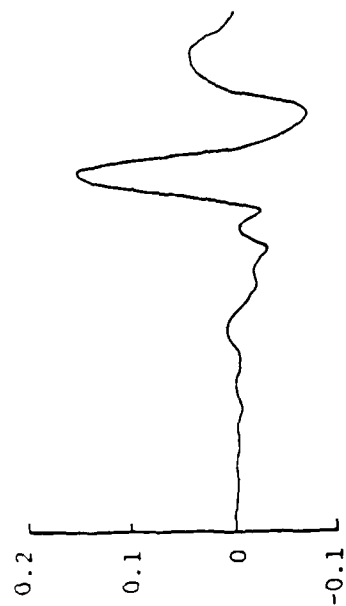


R = 156 m

Theory



R = 313 m



Observed

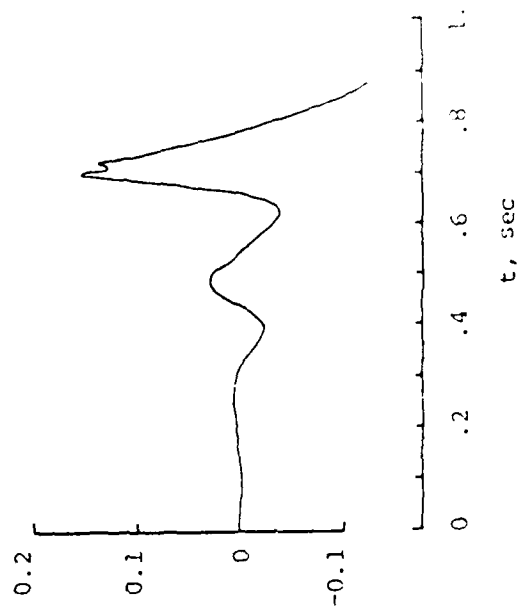
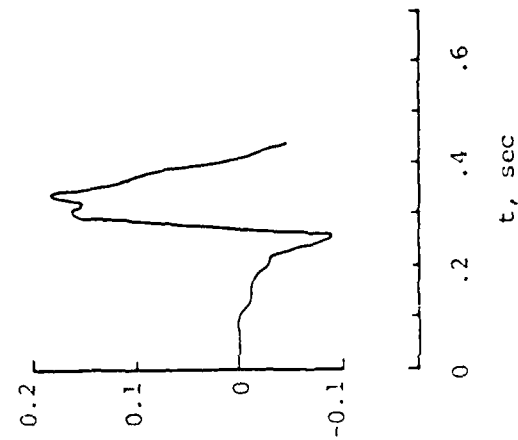
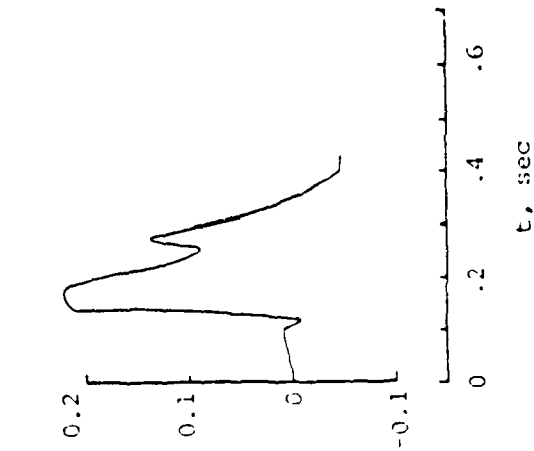


Figure 27. Comparison of predicted (top) and observed (bottom) vertical displacement waveforms for Pre-DIRECT COURSE, final site model.

ground motion parameters of interest. However, the basic scaling laws describing the variation of peak amplitude and dominant frequency with yield, range, site geology and instrument depth have already been inferred from the model and provide some preliminary basis for parametric analysis.

The principal assumptions underlying the theoretical scaling laws may be enumerated as follows:

- (1) The subsurface geology at the site of interest can be approximated as a sequence of homogeneous layers of constant thickness.
- (2) The source of the surface waves can be described by the linear response of the medium to the airblast loading on the surface outside the crater region (if any).
- (3) The yields of interest are sufficiently large that the surface wave motions will be dominated by frequency components near the corner frequency of the Rayleigh wave site response function, which coincides with the frequency of minimum group velocity and is given approximately by  $\beta/2H$  where  $H$  denotes the total soil thickness at the site and  $\beta$  is the average shear wave velocity of the soil column (Murphy and Bennett, 1980).
- (4) The observation point of interest is close enough to the source that the effects of anelastic attenuation on the propagating surface wave can be ignored to first order.

Given these assumptions, the surface wave peak amplitude,  $A$ , at a particular site is predicted to scale in the following manner.

- At a fixed observation distance (Murphy and Bennett, 1980):

$$A \sim W^{1/3}$$

- At a fixed yield, the amplitude decay with distance,  $r$ , is given approximately by the Airy phase attenuation law:

$$A \sim r^{-5/6}$$

- At a fixed scaled distance, it follows from the above two laws that:

$$A \sim W^{0.06}$$

Note that under the assumption that the surface wave is dominated by a pure sinusoidal component with constant frequency  $\beta/2H$ , these scaling laws apply to the velocity and acceleration, as well as the displacement, peak amplitudes.

The expected depth dependence of the surface wave motions can be analyzed in a preliminary fashion by employing the same approximations used in defining the other scaling laws. Let  $U_1(Z)$  and  $W_1(Z)$  denote the horizontal and vertical Rayleigh wave displacement components as a function of depth in the "surface layer". Then for cases in which the shear wave velocity ratio  $\beta_2/\beta_1 \lesssim 4$  we can write for frequency components near  $\beta_1/2H$  (Murphy and Hewlett, 1975):

$$\begin{aligned} \frac{W_1(Z)}{W_1(0)} = & \tilde{r}_{\alpha_1} \xi \gamma_1 \sinh \tilde{k} \tilde{r}_{\alpha_1} Z - (\gamma_1 - 1) \cosh \tilde{k} \tilde{r}_{\alpha_1} Z \\ & - \frac{\xi(\gamma_1 - 1)}{r_{\beta_1}} \sin k r_{\beta_1} Z + \gamma_1 \cos k r_{\beta_1} Z \end{aligned} \quad (6)$$

$$\begin{aligned} \frac{U_1(Z)}{iW_1(0)} = & - \xi \gamma_1 \cosh \tilde{k} \tilde{r}_{\alpha_1} Z + \frac{(\gamma_1 - 1)}{\tilde{r}_{\alpha_1}} \sinh \tilde{k} \tilde{r}_{\alpha_1} Z \\ & + \xi(\gamma_1 - 1) \cos k r_{\beta_1} Z + \gamma_1 r_{\beta_1} \sin k r_{\beta_1} Z \end{aligned} \quad (7)$$

where

$$\gamma_1 = 2 \left( \frac{\beta_1}{c} \right)^2 \quad (8)$$

$$k = \frac{\omega}{c} \quad (9)$$

$$r_{\beta_1} = \sqrt{c^2/\beta_1^2 - 1} \quad (10)$$

$$\tilde{r}_{\alpha_1} = \sqrt{1 - c^2/\alpha_1^2} \quad (11)$$

$$\xi = \left| \frac{U_1(0)}{W_1(0)} \right| \quad (12)$$

and  $c$  is the phase velocity at angular frequency  $\omega$ . For the nominal case in which  $\alpha = \sqrt{3} \beta$  and  $\beta_2 \approx 2\beta_1$ , it can be shown that at the Rayleigh wave characteristic frequency  $\omega \approx \pi\beta_1/H$ ,  $c/\beta_1 \approx 1.3$ ,  $\xi = 0.6$  and Equations (6) and (7) can be rewritten explicitly in the form:

$$\begin{aligned} \frac{W_1(Z)}{W_1(0)} &= 0.48 \sinh 1.43 \frac{Z}{H} - 0.21 \cosh 1.43 \frac{Z}{H} \\ &- 0.15 \sin 1.72 \frac{Z}{H} + 1.21 \cos 1.72 \frac{Z}{H} \end{aligned} \quad (13)$$

$$\begin{aligned} \frac{U_1(Z)}{iW_1(0)} &= -0.71 \cosh 1.43 \frac{Z}{H} + 0.31 \sinh 1.43 \frac{Z}{H} \\ &+ 0.12 \cos 1.72 \frac{Z}{H} + 0.98 \sin 1.72 \frac{Z}{H} \end{aligned} \quad (14)$$

The depth dependences predicted by these equations are shown in Figure 28 as a function of the dimensionless variable  $Z/H$ . It can be seen that, as

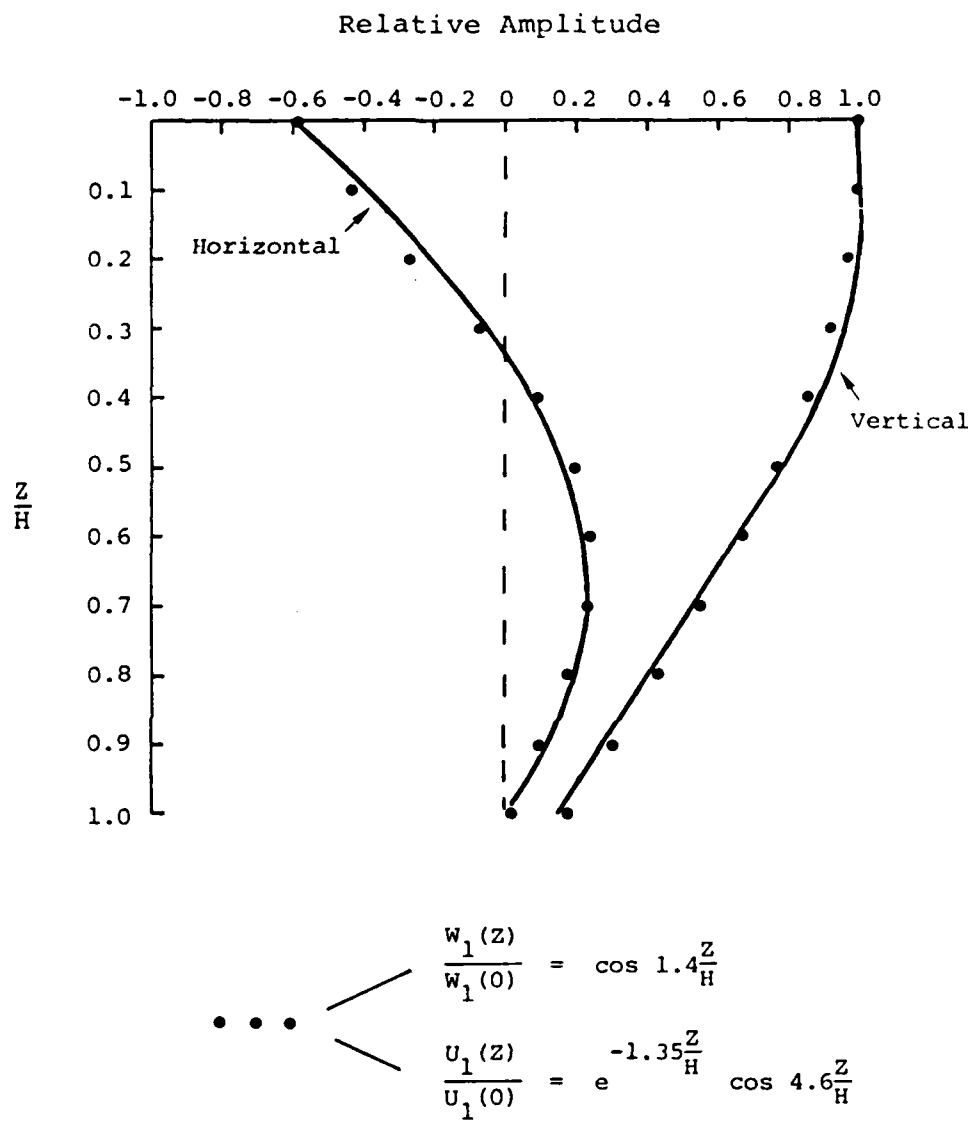


Figure 28. Predicted variation of surface wave amplitude with depth for the special case  $\beta_2/\beta_1 = 2$ ,  $\alpha = \sqrt{3} \beta$ ,  $f = \beta_1/2H$ .

in the case of the halfspace, the horizontal component of motion decreases to zero fairly rapidly (i.e., at  $Z \approx 0.35H$ ) and then changes sign. As is indicated on the figure, these depth dependences can be approximated quite closely by the following simple expressions.

$$\frac{w_1(Z)}{w_1(0)} = \cos 1.4 \frac{Z}{H} \quad (15)$$

$$\frac{u_1(Z)}{u_1(0)} \approx e^{-1.35 \frac{Z}{H}} \cos 4.6 \frac{Z}{H} \quad (16)$$

where  $|u_1(0)| \approx 0.6|w_1(0)|$ .

Preliminary indications are that the theoretically-based scaling laws proposed above are generally consistent with the large body of low frequency ground motion data which have been observed from both HE and nuclear atmospheric explosions (Personal Communication, C. J. Higgins, ARA, 1984). Work is currently in progress to perform more definitive comparisons with the available observations and to define the range of applicability of these approximate relations.

## SECTION 4

### CONCLUSIONS

#### 4.1 SUMMARY.

The investigations summarized in this report have centered on the simulation analysis of low frequency ground motions observed from atmospheric explosions and on the preliminary evaluation of a theoretically-based prediction methodology. In particular, the present effort has extended the previous research on low frequency ground motions from HE experiments to a full scale validation study conducted using data recorded from atmospheric nuclear explosions at NTS.

The mathematical model being used to simulate the low frequency ground motions produced by atmospheric explosions was briefly summarized in Section II and then applied to the theoretical simulation of ground motion data recorded from the NTS nuclear explosions TUMBLER I, UPSHOT-KNOTHOLE 10 and SMALL BOY. These three explosions represent a range of scaled HOB extending from about  $240 \text{ m/kt}^{1/3}$  (TUMBLER I) to essentially zero (SMALL BOY) and thus provide an opportunity to assess simulation capability over essentially the entire range of interest in ground motion vulnerability studies. The results of these simulations have confirmed the fact that the observed low frequency ground motions from such explosions can be accounted for by the airblast-induced Rayleigh wave. More specifically, these analyses have provided additional insight into the variation of the Rayleigh wave seismic source function with HOB. Thus, the simulation analysis of the ground motion data recorded from the near-surface SMALL BOY explosion confirmed the existence of an "exclusion radius" for such events, within which the incident airblast is not efficiently coupled into the Rayleigh wave radiation field due to energy dissipation associated with strong, nonlinear interaction effects. On the other hand, the evidence provided by the TUMBLER I and UPSHOT-KNOTHOLE 10 analyses indicated that this exclusion radius is effectively zero for explosions with significant HOB.

Some preliminary considerations concerning the prediction of low frequency ground motion parameters were addressed in Section III, where the experience gained with the Pre-DIRECT COURSE experiment was

assessed and some approximate scaling laws describing the dependence of low frequency ground motion characteristics on variables such as yield, distance, site geology and instrument depth were presented and discussed. It was found that the initial pre-shot prediction of the Pre-DIRECT COURSE low frequency ground motions was only partially successful, due to the fact that the subsurface geologic model available at that time was inaccurate. Subsequent analyses of the measured data, using a modified site model inferred from more extensive post-shot exploration, provided evidence which indicated that it should be possible to predict the low frequency ground motions produced by atmospheric explosions with good accuracy using the proposed theoretical model, if an accurate subsurface site model can be specified.

#### 4.2 CONCLUSIONS.

The analyses summarized above support the following conclusions regarding the low frequency ground motions observed from atmospheric nuclear explosions at NTS.

- (1) The low frequency components of the ground motions observed from these explosions can be accounted for by the airblast-induced Rayleigh waves. In fact, in the regime where the overpressure is less than about 100 kPa, this component of the motion was found to account for essentially all the significant observed particle velocity excursions with the exception of that associated with the overhead airslap-induced motion.
- (2) There is an "exclusion radius" associated with near-surface explosions, inside of which incident energy is not efficiently coupled into the surface wave mode of propagation. This radius has been shown to be effectively zero for explosions with significant HOB.

- (3) Much valuable ground motion data have been recorded from atmospheric nuclear explosions. However, these data need to be better documented and reprocessed using modern signal analysis techniques so that they can be more fully utilized in ground motion analysis studies.

With regard to development of procedures for predicting the characteristics of the low frequency ground motions produced by atmospheric explosions, results of studies conducted to date lead to the following conclusions.

- (1) The predicted surface wave characteristics are quite sensitive to the near-surface shear wave velocity structure at the site. Pre-DIRECT COURSE experience indicates that this velocity distribution cannot be adequately constrained on the basis of P wave refraction surveys.
- (2) For explosions which are large enough that the surface wave motions are dominated by frequency components near the corner frequency of the Rayleigh wave site response function (i.e.,  $f \approx \beta/2H$ ), the theoretical model predicts that the amplitude of the low frequency ground motion should vary with yield,  $W$ , as  $W^{1/3}$  and with range,  $R$ , approximately as  $R^{-5/6}$ .
- (3) If  $W(0)$ ,  $U(0)$  denote the vertical and horizontal component Rayleigh wave displacements on the surface, characterized by dominant frequency  $\beta/2H$ , then the corresponding displacements at depth  $Z$  within the surface layer of total thickness  $H$  can be approximated by the relations:

$$W(Z) = W(0) \cos 1.4 \frac{Z}{H}$$

(17)

$$U(Z) = U(0) e^{-1.35 \frac{Z}{H}} \cos 4.6 \frac{Z}{H}$$

## SECTION 5

### LIST OF REFERENCES

- Hawthorne, H. E. (1979), "Compilation of Local Fallout Data From Test Detonations 1945-1962 Extracted From DASA 1251 - Volume I: Continental U.S. Tests," DNA-1251-1-EX, DASIAC.
- Murphy, J. R. and R. A. Hewlett (1975), "Analysis of Seismic Response in the City of Las Vegas, Nevada: A Preliminary Microzonation," Bull. Seism. Soc. Am., 65, p. 1575.
- Murphy, J. R. (1978), "An Analysis of the Characteristics of Rayleigh Waves Produced by Surface Explosions," Final Technical Report to the Defense Nuclear Agency, DNA 4826F.
- Murphy, J. R. and T. J. Bennett (1980), "Analysis of the Low Frequency Ground Motion Environment For MX: Surface Waves and Valley Reverberation," Final Technical Report to Defense Nuclear Agency, DNA 5219F.
- Murphy, J. R., H. K. Shah and T. K. Tzeng (1981), "Analysis of the Low Frequency Ground Motion Environment For MX: Surface Waves From Multiple Explosions and Development of a Valley Reverberation Model," Final Technical Report to Defense Nuclear Agency, SSS-R-81-4934.
- Murphy, J. R., H. K. Shah and T. K. Tzeng (1982), "Analysis of Low Frequency Ground Motions Induced by Near-Surface and Atmospheric Explosions," Final Technical Report to Defense Nuclear Agency, DNA-TR-81-157.
- Sauer, F. (1958) "Ground Motion Produced by Aboveground Nuclear Explosions," unpublished.
- Speicher, S. J. and H. L. Brode (1981), "Airblast Overpressure Analytic Expression For Burst Height, Range and Time-Over an Ideal Surface," Pacific-Sierra Research Corporation, Note 385, November.
- Stubbs, C. T. (1977), "Redigitization and Superficial Analysis of the Ground Motion Data From Selected Surface Burst Nuclear Experiments," Final Technical Report to Defense Nuclear Agency, DNA 4088F.



## DISTRIBUTION LIST

### DEPARTMENT OF DEFENSE

ASSIST TO THE SECY OF DEF ATOMIC ENERGY  
ATTN: EXEC ASSIST

DEFENSE ADVANCED RSCH PROJ AGENCY  
ATTN: T BACHE

DEFENSE INTELLIGENCE AGENCY  
ATTN: DB-4C  
ATTN: RTS-2B  
ATTN: VP-TPO

DEFENSE NUCLEAR AGENCY  
2 CYS ATTN: SPAS G ULLRICH  
4 CYS ATTN: STTI-CA

DEFENSE TECHNICAL INFORMATION CENTER  
12 CYS ATTN: DD

FIELD COMMAND DNA DET 2  
LAWRENCE LIVERMORE NATIONAL LAB  
ATTN: FC-1

FIELD COMMAND DEFENSE NUCLEAR AGENCY  
ATTN: FCPR  
ATTN: FCTT  
ATTN: FCTT W SUMMA  
ATTN: FCTXE

UNDER SECY OF DEF FOR RSCH & ENGRG  
ATTN: STRAT & THEATER NUC FOR F VAJDA

### DEPARTMENT OF THE ARMY

U S ARMY ENGR WATERWAYS EXPER STATION  
ATTN: J STRANGE  
ATTN: J ZELASKO  
ATTN: LIBRARY  
2 CYS ATTN: WESSD J JACKSON  
ATTN: WESSE

### DEPARTMENT OF THE AIR FORCE

AIR FORCE GEOPHYSICS LABORATORY  
ATTN: LWH/H OSSING

AIR FORCE INSTITUTE OF TECHNOLOGY  
ATTN: LIBRARY

AIR FORCE OFFICE OF SCIENTIFIC RSCH  
ATTN: W BEST

AIR FORCE WEAPONS LABORATORY, AFSC  
ATTN: NTE M PLAMONDON  
ATTN: NTED J THOMAS  
ATTN: NTED R HENNY  
ATTN: SUL

AIR UNIVERSITY LIBRARY  
ATTN: AUL-LSE

FOREIGN TECHNOLOGY DIVISION, AFSC  
ATTN: NIIS LIBRARY

### DEPARTMENT OF ENERGY

UNIVERSITY OF CALIFORNIA  
LAWRENCE LIVERMORE NATIONAL LAB  
ATTN: L-221 D GLENN  
ATTN: L-53 TECH INFO DEPT LIB

LOS ALAMOS NATIONAL LABORATORY  
ATTN: MS P364 RPT LIB

SANDIA NATIONAL LABORATORIES  
ATTN: LIB & SEC CLASS DIV

SANDIA NATIONAL LABORATORIES  
ATTN: ORG 7111 L HILL  
ATTN: ORG 7112 A CHABAI  
ATTN: TECH LIB 3141

### OTHER GOVERNMENT

CENTRAL INTELLIGENCE AGENCY  
ATTN: OSWR/NED

### DEPARTMENT OF DEFENSE CONTRACTORS

AEROSPACE CORP  
ATTN: LIB ACQ M1/199

APPLIED RESEARCH ASSOCIATES, INC  
ATTN: N HIGGINS

APPLIED RESEARCH ASSOCIATES, INC  
ATTN: S BLOUIN

APPLIED RESEARCH ASSOCIATES, INC  
ATTN: D PIEPENBURG

APPLIED RESEARCH ASSOCIATES, INC  
ATTN: R FRANK

BDM CORP  
ATTN: F LEECH

BOEING CO  
ATTN: M/S 8K-22 D CHOATE

CALIFORNIA RESEARCH & TECHNOLOGY, INC  
ATTN: K KREYENHAGEN  
ATTN: LIBRARY  
ATTN: M ROSENBLATT  
ATTN: S SCHUSTER

CALIFORNIA RESEARCH & TECHNOLOGY, INC  
ATTN: F SAUER

KAMAN SCIENCES CORP  
ATTN: LIBRARY

**DEPT OF DEFENSE CONTRACTORS (CONTINUED)**

KAMAN TEMPO  
ATTN: DASAC

KAMAN TEMPO  
ATTN: DASAC

MAXWELL LABORATORIES, INC  
ATTN: J MURPHY

MERRITT CASES, INC  
ATTN: J MERRITT  
ATTN: LIBRARY

NEW MEXICO ENGINEERING RESEARCH INSTITUTE  
ATTN: N BAUM

PACIFIC-SIERRA RESEARCH CORP  
ATTN: H BRODE, CHAIRMAN SAGE

R & D ASSOCIATES  
ATTN: C K B LEE  
ATTN: D SIMONS  
ATTN: J LEWIS  
ATTN: P HAAS  
ATTN: TECH INFO CTR

R & D ASSOCIATES  
ATTN: G GANONG

RAND CORP  
ATTN: P DAVIS

RAND CORP  
ATTN: B BENNETT

S-CUBED  
ATTN: D GRINE  
2 CYS ATTN: H SHAH

2 CYS ATTN: J DERMENGIAN  
2 CYS ATTN: J MURPHY  
ATTN: LIBRARY  
ATTN: T RINEY

SCIENCE APPLICATIONS INTL CORP  
ATTN: TECHNICAL LIBRARY

SCIENCE APPLICATIONS INTL CORP  
ATTN: D MAXWELL

SCIENCE APPLICATIONS INTL CORP  
ATTN: W LAYSON

SOUTHWEST RESEARCH INSTITUTE  
ATTN: A WENZEL

SRI INTERNATIONAL  
ATTN: D KEOUGH

TERRA TEK, INC  
ATTN: S GREEN

TRW ELECTRONICS & DEFENSE SECTOR  
2 CYS ATTN: N LIPNER  
ATTN: P BHUTA  
ATTN: TECH INFO CTR

WEIDLINGER ASSOC, CONSULTING ENGRG  
ATTN: T DEEVY

WEIDLINGER ASSOC, CONSULTING ENGRG  
ATTN: M BARON

WEIDLINGER ASSOC, CONSULTING ENGRG  
ATTN: J ISENBERG

END

DTic

7-86